Developing Inhibitors of the p47phox-p22phox Protein-Protein Interaction by Fragment-Based Drug Discovery

Solbak, Sara Marie Øie; Zang, Jie; Narayanan, Dilip; Høj, Lars Jakobsen; Bucciarelli, Saskia; Softley, Charlotte; Meier, Sebastian; Langkilde, Annette Eva; Gotfredsen, Charlotte Held; Sattler, Michael

Total number of authors:
11

Published in:
Journal of Medicinal Chemistry

Link to article, DOI:
10.1021/acs.jmedchem.9b01492

Publication date:
2020

Document Version
Publisher's PDF, also known as Version of record

Journal of Medicinal Chemistry

pubs.acs.org/jmc

Article

Developing Inhibitors of the p47phox–p22phox Protein–Protein Interaction by Fragment-Based Drug Discovery

Sara Marie Øie Solbak, Jie Zang, Dilip Narayanan, Lars Jakobsen Høj, Saskia Bucciarelli, Charlotte Softley, Sebastian Meier, Annette Eva Langkilde, Charlotte Held Gotfredsen, Michael Sattler, and Anders Bach*

Cite This: https://dx.doi.org/10.1021/acs.jmedchem.9b01492

Read Online

ACCESS | Metrics & More | Article Recommendations | Supporting Information

ABSTRACT: Nicotinamide adenine dinucleotide phosphate oxidase isoform 2 is an enzyme complex, which generates reactive oxygen species and contributes to oxidative stress. The p47phox–p22phox interaction is critical for the activation of the catalytical NOX2 domain, and p47phox is a potential target for therapeutic intervention. By screening 2500 fragments using fluorescence polarization and a thermal shift assay and validation by surface plasmon resonance, we found eight hits toward the tandem SH3 domain of p47phox (p47phox^{SH3A-B}) with K_D values of 400–600 μM. Structural studies revealed that fragments **1** and **2** bound two separate binding sites in the elongated conformation of p47phox^{SH3A-B} and these competed with p22phox for binding to p47phox^{SH3A-B}. Chemical optimization led to a dimeric compound with the ability to potently inhibit the p47phox^{SH3A-B}–p22phox interaction (K_i of 20 μM). Thereby, we reveal a new way of targeting p47phox and present the first report of drug-like molecules with the ability to bind p47phox and inhibit its interaction with p22phox.

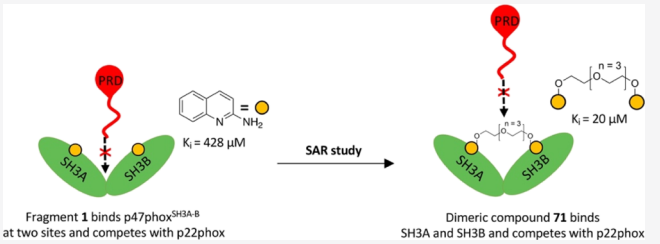

INTRODUCTION

The multi-subunit enzyme complex nicotinamide adenine dinucleotide phosphate (NADPH) oxidase isoform 2 is highly expressed in phagocytes, where it catalyzes the reduction of molecular oxygen to the superoxide anion ($O_2^{\bullet-}$). This reactive oxygen species (ROS) generating enzyme is known to have a key role in innate immunity, as demonstrated in chronic granulomatous disease (CGD) caused by an inherited deficiency in one of the NADPH oxidase 2 subunits, where the phagocytes fail to kill invading microorganisms.[1] Excessive ROS production by NADPH oxidase 2 on the other hand contributes to oxidative stress and is connected to a wide range of diseases involving inflammation, diabetes, and cancer.[2,3] Furthermore, NADPH oxidases contribute to brain damage in relation to traumatic brain injury, reperfusion injury in stroke, and neurodegenerative diseases.[1,3−5]

The NADPH oxidase 2 complex comprises a membrane-bound flavocytochrome b558, a heterodimer of the catalytically active NOX2 domain and p22phox, three cytosolic proteins, p40phox, p47phox and p67phox, and a small G protein Rac GTPase.[3,6] NOX2 is activated by Ca^{2+}-influx activating the phosphokinase C (PKC), which further phosphorylates C-terminal serine residues located in the autoinhibitory region (AIR) and the proline-rich region of p47phox.[4,7] The phosphorylation causes a conformational change of p47phox, allowing the cytosolic proteins to relocate to the plasma membrane, where they associate with flavocytochrome b558, forming the active NADPH oxidase 2 complex. In its inactive state, the p47phox tandem Src homology 3 (SH3) domain (SH3A–B) is occupied by the AIR of p47phox. However, upon p47phox phosphorylation in the AIR domain, the conformational change involves the detachment of the AIR domain from the SH3A–B domain, allowing SH3A–B to bind to the proline-rich domain (PRD) of p22phox instead (Figure 1).[8] The truncated p47phox SH3A–B (p47phox$^{151-286}$)

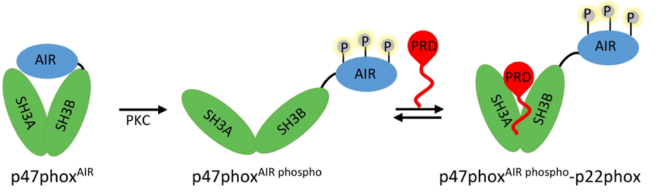

Figure 1. p47phox–p22phox binding model. PKC activates p47phox^{AIR} by phosphorylating seven C-terminal serine residues (three in the AIR domain), leading to a conformational change, where the AIR domain is removed from the tandem SH3 domain allowing binding to the PRD of p22phox.

Received: September 8, 2019
Published: January 10, 2020

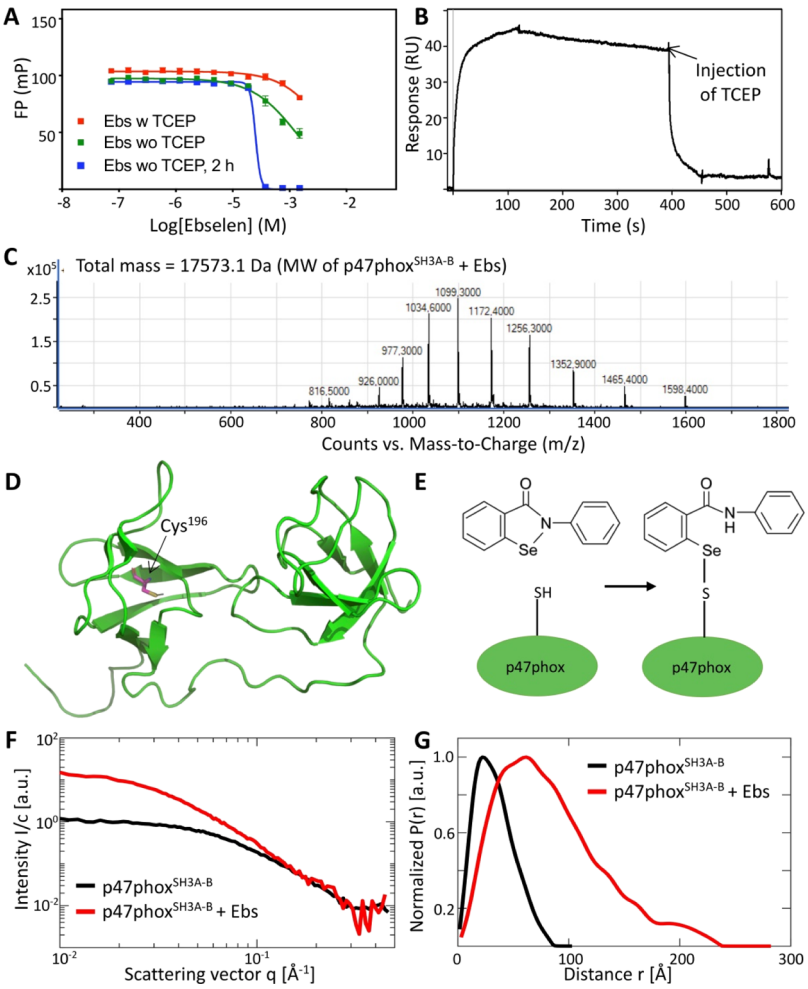

Figure 2. Interaction of p47phox^{SH3A-B} with ebselen. (A) Ebselen tested in the FP competition assay using the Cy5-p22phox$^{149-162}$ probe in the absence of TCEP—after 10 min (green) or 2 h (blue) incubation—and in the presence of TCEP (red). (B) SPR sensorgram of ebselen (12.5 μM) injected over 4684 RU-immobilized p47phox^{SH3A-B} on a biosensor chip followed by abrogation of the complex by 2 mM TCEP. (C) LC−MS data of 0.2 mg/mL p47phox^{SH3A-B} with 200 μM ebselen showing a total mass of 17573.1 ± 0.5 Da. (D) Solution NMR structure of p47phox^{SH3A-B} in complex with p22phox$^{149-168}$ (PDB ID: 1WLP); Cys^{196} in the SH3A domain is highlighted (purple), while the p22phox peptide is removed. (E) Our data suggest that ebselen forms a selenylsulphide bond with Cys^{196} of p47phox^{SH3A-B} forming a stable complex. (F) SAXS data for p47phox^{SH3A-B} (black) and p47phox^{SH3A-B} in the presence of ebselen (red) plotted as concentration-normalized scattering intensity $I(q)/c$ in arbitrary units vs q and (G) corresponding pair-distance distribution function $P(r)$.

without the AIR (here referred to as p47phox^{SH3A-B}) is considered a model protein of activated p47phox, as it has an open tandem SH3 domain and does not require phosphorylation to bind to p22phox.[8,9] The structure of the tandem SH3 domain including the AIR (p47phox$^{151-342}$; here referred to as p47phox^{AIR}) and p47phox^{SH3A-B} in complex with the p22phox-derived peptide p22phox$^{149-168}$ have previously been investigated by X-ray crystallography, nuclear magnetic resonance (NMR), and small-angle X-ray scattering (SAXS).[8−12] By X-ray crystallography, both p47phox^{AIR} and p47phox^{SH3A-B} in complex with p22phox$^{149-168}$ were found to form intertwined dimers.[8,12] However, in solution both proteins were found by NMR and SAXS analysis to be monomeric.[9,10] Interestingly, the SAXS studies revealed an overall more compact conformation of the p47phox^{SH3A-B}–p22phox complex than for the extended apo p47phox^{SH3A-B}. Furthermore, the binding interface of p47phox^{SH3A-B} to p22phox$^{149-168}$ was characterized by NMR chemical shift perturbation (CSP) analysis based on ^{1}H−^{15}N HSQC NMR titration experiments. In particular, for the three tryptophan residues in SH3A (Trp^{193}, Trp^{194}, and Trp^{204}) and the two in SH3B (Trp^{263} and Trp^{264}), significant CSPs were observed during titration with p22phox$^{149-168}$. This finding reflects that p22phox$^{149-168}$ stably interacts with a region composed by both SH3 domains forming a crevice in the middle of the tandem SH3 domain, as shown by NMR structure determination (PDB ID: 1WLP).[9]

The binding between p47phox and p22phox is essential for NOX2 activation, and p47phox has thus been suggested as a target for therapeutic intervention.[4,13] This approach has the potential to provide novel, specific, and genuine NOX2 inhibitors, which have been shown to be notoriously difficult to develop by other strategies.[14] However, the only small molecular compounds reported to prevent NADPH oxidase 2 activity by direct inhibition of the p47phox−p22phox interaction are ebselen (2-phenyl-1,2-benzisoselenazol-3(2*H*)-one) and a series of close analogues.[13] Ebselen is a synthetic seleno-organic ROS scavenging compound known to induce cysteine-targeted oxidation followed by S-thiolation—an

https://dx.doi.org/10.1021/acs.jmedchem.9b01492
J. Med. Chem. XXXX, XXX, XXX−XXX

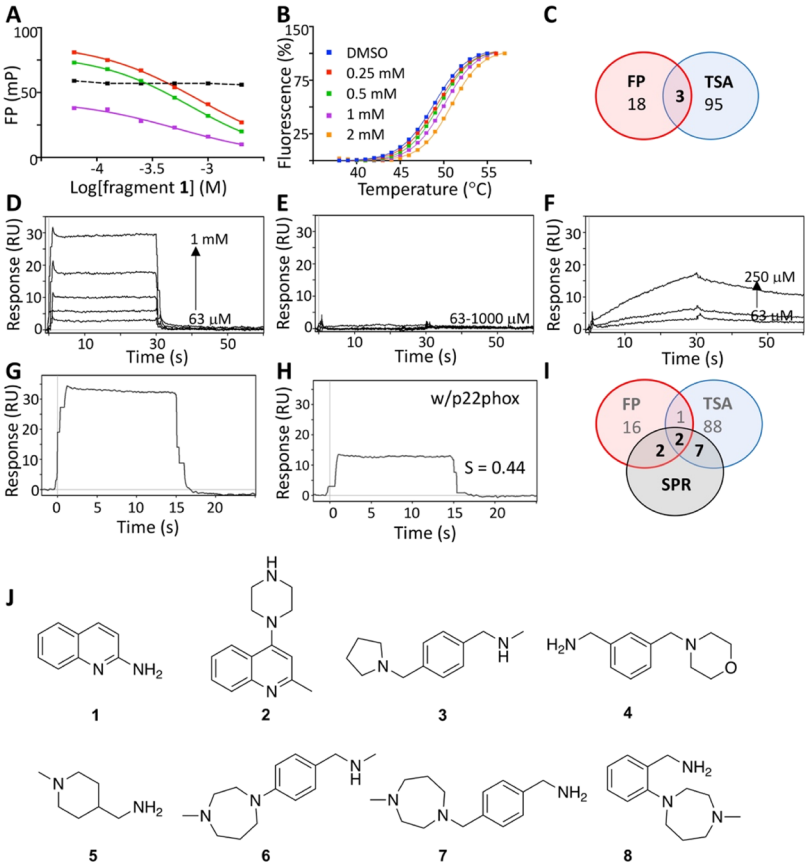

Figure 3. Fragment screening and validation. (A) FP assay for fragment hit **1** competing with the fluorescent probe Cy5-p22phox$^{149-162}$ (red) and TAMRA-p22phox$^{151-162}$ (purple) for binding to p47phox^{SH3A-B}. The assay was also performed in the presence of 0.01% Triton-X (green) and without protein (black). (B) TSA melting curves for p47phox^{SH3A-B} with various concentrations of **1**. (C) Venn diagram of validated screen hits from FP and TSA. (D–F) Validated FP and TSA hits were injected over immobilized p47phox^{SH3A-B} and evaluated by SPR. Fragments showing a concentration-dependent binding response and a fragment-like binding kinetic (as **1**, D) were confirmed as hits. Fragments showing no binding up to 1 mM (as example in E) or a nonfragment-like binding behavior (as in F) were not regarded as true hits. (G,H) Hits confirmed by SPR were further investigated in an SPR inhibition assay by injecting 1 mM fragment over immobilized p47phox^{SH3A-B} (3358 RU) in the absence (G) and presence (H) of 10 μM p22phox$^{149-168}$ in the running buffer. (I) Venn diagram of final validated screen hits from FP, TSA, and SPR (J) Chemical structures of the eight fragments selected for further investigations.

oxidative reversible modification of the cysteine residues of proteins.[15]

In this study, we show that ebselen binds p47phox^{SH3A-B} covalently, leading to destabilization and aggregation of the protein—a mechanism that is not promising for further drug development. Instead, to find novel reversible inhibitors of the p47phox–p22phox interaction, we used a fragment-based drug discovery (FBDD) approach. We thereby identified several small-molecules binding to the p47phox^{SH3A-B}, the best ones being dimeric compounds which display a 13–30-fold higher affinity relative to the parent fragment hits.

RESULTS AND DISCUSSION

Assay Development and Mechanism of Ebselen. In order to discover small molecular inhibitors of the p47phox–p22phox interaction, we developed a fluorescence polarization (FP) inhibition assay, a thermal shift assay (TSA), and a surface plasmon resonance (SPR) binding assay, which were validated by testing the p22phox derived peptides p22phox$^{151-162}$, p22phox$^{149-168}$, and p22phox$^{149-162}$, all containing the PRD known to bind p47phox^{SH3A-B}. The binding affinity of the p22phox peptides to p47phox^{SH3A-B} determined from FP and SPR corresponded to literature values,[8,9,13] and TSA showed increased melting temperatures indicative of binding (Supporting Information Figures S1–S3 and Table S1). According to the literature, SPR binding experiments of p22phox peptides to p47phox^{AIR} gave a clear reduced binding affinity (Supporting Information Figure S3D,E and Table S1).[8,16]

Ebselen was found to prevent NOX2 activation by inhibiting the interaction between p47phox and p22phox, as shown by FP.[13] We, therefore, considered if ebselen could be a useful reference compound for our assays and investigated the mechanism of action in more detail. In FP, ebselen in the absence of the reducing agent tris-(2-carboxyethyl)phosphine (TCEP) yielded a K_i of 63 ± 6 μM, while a >10-fold increase in K_i (>300 μM) was observed with TCEP present in the buffer, which indicate a covalent binding mode. When prolonging the incubation time from 10 min to 2 h in the FP assay without TCEP, the K_i was reduced to 12 ± 0.07 μM (Figure 2A). In SPR, ebselen strongly bound p47phox^{SH3A-B} with an almost nonreversible binding kinetic (slow dissociation rate) (Figure 2B). The binding was however reversed by TCEP (Figure 2B and Supporting Information Figure S4A). Also, LC–MS analysis of p47phox^{SH3A-B} with ebselen showed a total mass of 17,573.1 Da (Figure 2C), which compared to the mass of p47phox^{SH3A-B} without ebselen (17,299.5 Da)

https://dx.doi.org/10.1021/acs.jmedchem.9b01492
J. Med. Chem. XXXX, XXX, XXX–XXX

Table 1. Biophysical Data of the Final 8 Validated Fragments[a]

Compds	Compd identity	MW	ΔT_m(°C) (0.25/0.5/1/2 mM)	K_i (μM)[b]	K_D (μM)[b]	S[c]
1	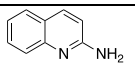	144.2	0.3/0.6/1.2/2.0	428 ± 23	488 ± 130	0.61 ± 0.2
2	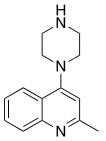	227.3	0.7/1.4/2.1/3.6	606 ± 25	412 ± 130	0.48 ± 0.1
3	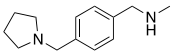	204.3	0.4/0.4/1.7/3.0	No hit	465 ± 160	0.25 ± 0.07
4	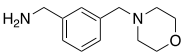	206.3	1.0/0.9/1.4/2.2	No hit	563 ± 320	0.38 ± 0.2
5	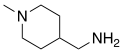	128.2	0.8/0.8/0.9/2.4	No hit	349 ± 29	0.75 ± 0.3
6	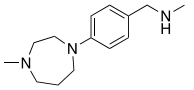	233.4	0.6/0.8/1.6/2.9	No hit	548 ± 160	0.22 ± 0.05
7	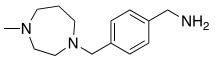	233.4	0.5/0.3/1.1/2.0	No hit	418 ± 83	0.36 ± 0.06
8	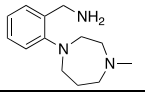	219.3	-0.1/0.3/0.9/1.4	No hit	504 ± 110	0.35 ± 0.10

[a]ΔT_m was calculated from TSA data, K_i from FP, steady state affinities (K_D) from SPR sensorgrams seen in Supporting Information Figure S6. [b]K_i and K_D values are reported as the mean ± SEM ($n \geq 3$). [c]S values are reported as mean ± SEM ($n = 2$).

(Supporting Information Figure S4B) corresponds to a mass-increase similar to the molecular weight (MW) of ebselen (274.2 Da). These results demonstrate a covalent interaction of ebselen with the only cysteine (Cys^{196}) of $p47phox^{SH3A-B}$ (Figure 2D−E). Furthermore, SAXS studies indicated aggregation of $p47phox^{SH3A-B}$ in the presence of ebselen, evident by a strong increase in the maximum dimension of the particles (D_{max}) (starting at 235 Å, compared to the 86 Å without ebselen). The corresponding SAXS-derived radius of gyration (R_g = 67.6 Å) and the concentration-normalized scattering intensity at q = 0 ($I(0)/c$ = 17.2 a.u) were also higher than without ebselen (26.5 Å and 1.1 a.u, respectively) (Figure 2F−G and Supporting Information Table S2). The aggregation was observed shortly after sample preparation and increased over time (data not shown).

Thus, ebselen inhibits NOX2 by covalent binding to Cys^{196} of $p47phox^{SH3A-B}$, leading to destabilization and aggregation of $p47phox^{SH3A-B}$, rather than by occupying the p22phox binding pocket. This dramatic effect can be explained by Cys^{196} being localized directly adjacent to residues Trp^{193}, Trp^{204}, Phe^{195}, and Val^{186}, reported to form the hydrophobic binding pocket for p22phox in the p47phox SH3A domain.[9] Although this mechanism of action of ebselen prevents p47phox from binding to p22phox, resulting in reduced NOX2 activity as described,[13] and ebselen may have some promise as a drug candidate,[17−19] such a mechanism does not seem useful for a chemical probe,[20] as it likely comes with unspecific effects. Indeed, ebselen has been found active against a wide range of proteins, and is thus a nonselective compound.[15,21] Based on this, we used the $p22phox^{151-162}$ and $p22phox^{149-168}$ peptides as assay controls.

Fragment Screening and Hit Validation. To develop direct inhibitors of the p47phox−p22phox interaction, 2500 rule of 3 compliant fragments[22] were screened at 1 mM for binding to $p47phox^{SH3A-B}$ in the FP assay using the p22phox-derived Cy5 probe (Cy5-$p22phox^{149-162}$), and at 0.5 mM for inducing thermal stabilization of $p47phox^{SH3A-B}$ by TSA. The FP screening resulted in 75 fragments (3.0% hit rate) that caused at least a 20% decrease in polarization relative to the dimethyl sulfoxide (DMSO) control. The TSA screen resulted in 109 fragment hits (4.4% hit rate), where a hit was defined as a fragment that induced a ΔT_m > 0.9 °C relative to the negative control, and a sigmoidal melting curve with a fluorescence window in the proximity of the controls.

The 75 hits from the primary FP screen were validated in a 6-point FP dose−response experiment (63 μM−2 mM) in the absence and presence of 0.01% Triton-X to exclude aggregation-based promiscuous inhibitors.[23] The fragments were also tested using the TAMRA-probe (TAMRA-$p22phox^{151-162}$), in the absence of $p47phox^{SH3A-B}$, and by assessing the stability of the total fluorescence intensity (FLINT), in order to remove false-positives because of fluorescence inner-filter effects.[24] A total of 22 fragments had positive results in at least three out of four tests and were selected as validated FP hits (0.9% hit rate) (the FP validation data for **1** are shown in Figure 3A). The hits from the primary TSA screen were validated in a 4-point TSA dose−response experiment (0.25−2 mM). A total of 98 fragments (3.9% hit rate) showed a dose-dependent increment in ΔT_m, and were thus considered validated TSA hits (the TSA data for **1** are shown in Figure 3B). Only three hits were validated in both FP and TSA. A low number of common hits is often seen in fragment screening studies and is likely due to the underlying assay principles and sensitivities.[25−27]

Twenty-four of the validated fragments contained potentially reactive groups, such as thiourea and nitriles, or had structural similarity to ebselen. In analogy to ebselen, one fragment, (2-(3-(trifluoromethyl)phenyl)isothiazol-3(2*H*)-one) showed a mass increase in LC−MS equal to the MW of the fragment (245.2 Da), indicating covalent binding, so this was removed from further studies leaving 116 fragment hits validated in FP or TSA (Figure 3C).

https://dx.doi.org/10.1021/acs.jmedchem.9b01492
J. Med. Chem. XXXX, XXX, XXX−XXX

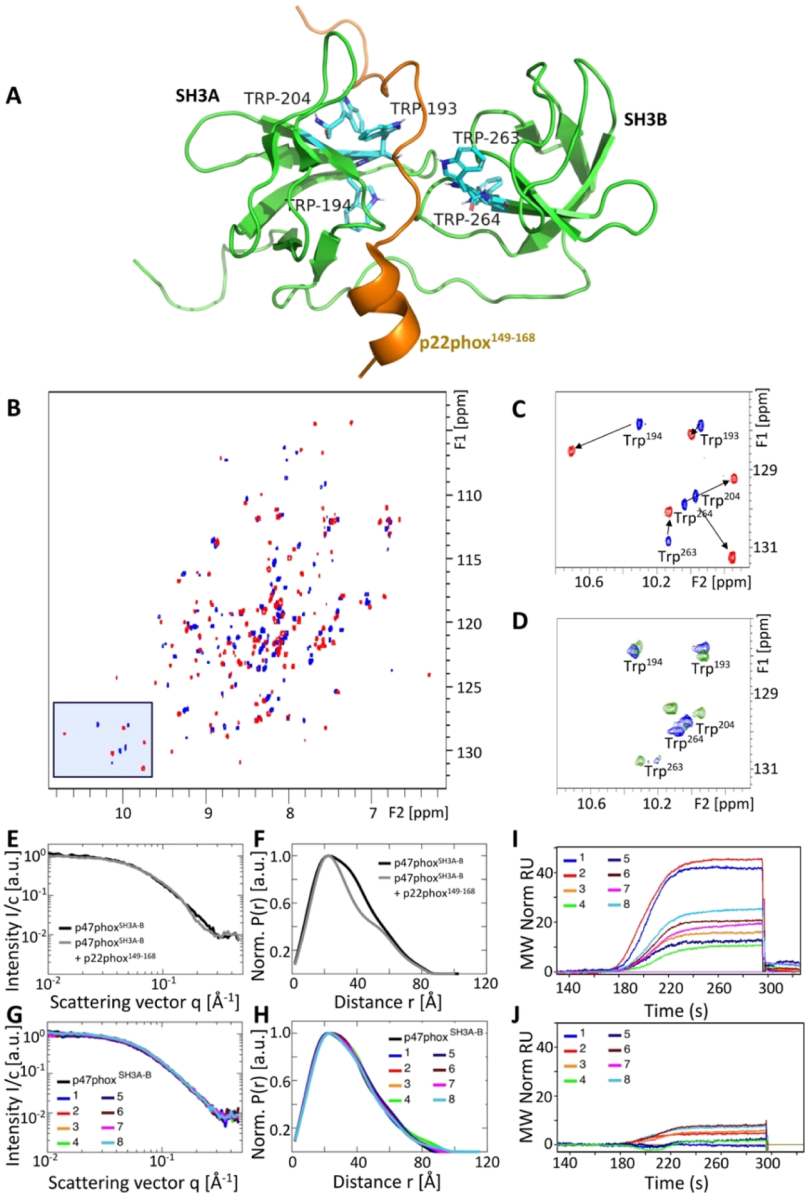

Figure 4. Validation of fragment hits by NMR, SAXS, and SPR binding stoichiometry. (A) Solution NMR structure of p47phox^{SH3A-B} (green) in complex with p22phox$^{149-168}$ (orange) (PDB ID: 1WLP), where the five Trp indole NH groups of p47phox^{SH3A-B} situated in the binding pocket are highlighted. (B) $^{1}H-^{15}N$ HSQC spectra of p47phox^{SH3A-B} free (blue) and in the presence of 4-fold molar excess of p22phox$^{149-168}$ (red). (C) Expanded region with indole NH signals of the five tryptophan residues in p47phox^{SH3A-B} free (blue) and bound to p22phox$^{149-168}$ (red). (D) Same expanded tryptophan indole NH region of p47phox^{SH3A-B} free (blue) superimposed with p47phox^{SH3A-B} in the presence of fragment hit **1** (1:20) (green), both samples supplemented with 4% DMSO. (E) SAXS data for p47phox^{SH3A-B} (black) and p47phox in the presence of p22phox$^{149-168}$ (grey) plotted as the concentration-normalized scattering intensity $I(q)/c$ in arbitrary units vs q and (F) corresponding pair-distance distribution function $P(r)$. (G) SAXS data for p47phox^{SH3A-B} (black) and p47phox^{SH3A-B} in the presence of fragments plotted as the concentration-normalized scattering intensity $I(q)/c$ in arbitrary units vs q and (H) corresponding pair-distance distribution function $P(r)$. (I) 8 final fragment hits were injected by a one-step gradient injection over immobilized p47phox^{SH3A-B} (2745 RU) to distinguish the differences in the MW-normalized response maximum binding level by SPR. (J) SPR inhibition assay where p22phox$^{149-168}$ was injected constantly at 10 μM while injecting a one-step gradient of 1 mM fragment over immobilized p47phox^{SH3A-B}.

Fragment Binding to p47phox^{SH3A-B} Characterized by SPR. The 116 validated hits were further assayed for direct binding to p47phox^{SH3A-B} by SPR, where the fragments were injected in two-fold serial dilutions over p47phox^{SH3A-B} immobilized on the biosensor chip. Seventy-two fragments showed a concentration-dependent response, thus confirming interaction with p47phox^{SH3A-B} (SPR data of **1** are shown in Figure 3D), while 39 fragments displayed low or no binding and five fragments showed nonfragment-like binding with slow on- or off-rates (see examples in Figure 3E–F).

To evaluate whether the 72 SPR-validated fragments bind to or interfere with the binding interface of p22phox at p47phox, we performed an SPR inhibition assay.[28] The fragments (1 mM) were injected over immobilized p47phox^{SH3A-B}, where the binding interface between p47phox^{SH3A-B} and p22phox was blocked by including p22phox$^{149-168}$ at saturating concentration (10 μM) in the running and ligand buffer.

https://dx.doi.org/10.1021/acs.jmedchem.9b01492
J. Med. Chem. XXXX, XXX, XXX−XXX

Following this assay, a similar injection was performed over the p47phox^{SH3A-B} surface not blocked by p22phox$^{149-168}$. A reduced binding of the fragments to p47phox^{SH3A-B} blocked by p22phox, would indicate that the fragments bind to the same interface at p47phox^{SH3A-B} as p22phox. Out of the 72 tested fragments, 14 showed a reduced binding response in the inhibition assay, with a calculated metric $S \geq 0.15$, corresponding to a reduction in the response level of ~25% (data for p22phox$^{151-162}$ and fragment **1** are shown in Supporting Information Figure S5 and Figure 3G−H, respectively). The 14 fragment hits were checked for structural similarities to known pan-assay interference compounds (PAINS) or aggregators using the filtering tool FAFdrugs4 (Free ADME−Tox Filtering Tool)[29] and Aggregator Advisor.[30] One fragment containing a thioketone was flagged as a potential covalent binder. The SPR binding experiments and inhibition assays of the remaining 13 hits were repeated in order to confirm these. Two of the fragments showed only little reduction in binding in the presence of the blocking peptide and were excluded, resulting in 11 SPR validated hits (cf. Venn diagram in Figure 3I). Out of these, three had very weak affinities to p47phox, and thus eight fragments (Figure 3J) were selected for further investigations by NMR and SAXS. SPR sensorgrams and biophysical data for these are shown in Supporting Information Figure S6 and Table 1.

NMR Chemical Shift Changes in p47phox^{SH3A-B} upon Fragment Binding. The SPR inhibition assay shows that p22phox reduces binding of the fragments, which indicates that our fragment hits bind to the same site of p47phox^{SH3A-B} as p22phox. To explore this further, we analyzed the CSPs in $^{1}H-^{15}N$ HSQC spectra focusing on the five Trp key residues considered in the binding interface of p47phox^{SH3A-B} to p22phox (Figure 4A).[9] As described in the literature, large chemical shift changes with slow exchange at the NMR chemical shift time scale were observed for all five well-resolved Trp indole NHs of p47phox^{SH3A-B} when titrated with p22phox$^{149-168}$ (p47phox^{SH3A-B}−p22phox$^{149-168}$ ratios 1:0, 2:1, 1:1, 1:2 and 1:4) (Figure 4B,C and Supporting Information Figure S7). The assignment of the Trp indole signals of p47phox^{SH3A-B} in complex with p22phox$^{149-168}$ was obtained from Ogura et al.,[9] and the tentative assignment of Trp indole signals of the free p47phox^{SH3A-B} was derived from titration experiments with p22phox$^{149-168}$ (Supporting Information Figure S7). Subsequently, titrations with all eight fragment hits were performed (p47phox^{SH3A-B}:fragment ratio 1:0, 1:5, 1:10, and 1:20) and the absolute CSP measured for the indole NH signals during titrations with each of the fragments were characterized (Figure 4D, Supporting Information Figure S8 and Table S3). All CSPs of the indole NHs of p47phox^{SH3A-B} upon titration of p22phox$^{149-168}$ reflect binding in slow exchange. Fragment hits **1** and **2** were the only fragments showing CSPs for all five indole NHs of the Trps, including strong CSPs with slow to intermediate exchange binding kinetics for Trp residues Trp^{193}, Trp^{194} Trp^{204}, Trp^{263}, and Trp^{264} situated both in the SH3A and SH3B region of p47phox^{SH3A-B} (Supporting Information Table S3 and Figure S8A,B). Fragment hits **4**, **5**, and **7** showed only weak CSP for one Trp indole NH (Trp^{193}) located in the SH3A domain, thus indicative of little influence on the magnetic environment of the indole NHs of p47phox^{SH3A-B} upon binding to these fragments and binding to only the SH3A domain (Supporting Information Figure S8G−I,M). Fragment hits **3**, **6**, and **8** showed CSPs of three or four indole NHs, mostly characterized as weak.

Solution Structure of p47phox^{SH3A-B} upon Fragment Binding Investigated by SAXS. p22phox-peptides have been shown by Ogura et al.[9] and Yuzawa et al.[10] to bind a compact conformation of p47phox^{SH3A-B}. To explore if our eight fragment hits bound in a similar manner, we studied the overall structure and conformation of p47phox^{SH3A-B} and the auto-inhibited form p47phox^{AIR} by SAXS studies. The pair-distance distribution functions of the SAXS data of p47phox^{SH3A-B} when binding to p22phox$^{149-168}$ and p22phox$^{151-162}$ are narrower (Figure 4E,F and Supporting Information Figure S9A,B) and the Kratky plots are more bell-shaped (Supporting Information Figure S9C) than for the free p47phox^{SH3A-B}, thus indicating a more compact conformation of p47phox^{SH3A-B} when binding to p22phox peptides and supporting the conclusions of Ogura et al.[9] A similar compact conformation was observed for p47phox^{AIR} compared to p47phox^{SH3A-B} (Supporting Information Figure S9D−F and Table S2), as shown by Yuzawa et al.[10] Possible alterations of p47phox^{AIR} upon the addition of p22phox-derived peptides were not previously investigated; however, our data did not indicate any differences between p47phox^{AIR} with and without p22phox$^{149-168}$ (Supporting Information Figure S9D−F and Table S2). In contrast to the p22phox peptides, no significant conformational changes in p47phox^{SH3A-B} were observed with any of the eight fragments at either 2 or 4 mM (Figure 4G,H). One fragment with high solubility (fragment hit **8**) was tested also at a 10 mM concentration, showing no difference between any of the concentrations (data not shown). These SAXS data indicate that the fragments bind to an extended conformation of p47phox^{SH3A-B}.

SPR Binding Level as a Measure to Elucidate Binding Stoichiometry. The NMR experiments of p47phox^{SH3A-B} with the fragment hits **1** and **2** show the influence of fragments binding on chemical shifts of Trp residues in both the SH3A and SH3B domains of p47phox. The SAXS data show that all fragments bind to an extended conformation of p47phox^{SH3A-B}, and not a compact conformation as induced upon p22phox binding. This means that the SH3A and SH3B domains of p47phox^{SH3A-B} are not close enough in space to form a joint extended binding pocket accommodating fragment hits **1** and **2**, which would explain the chemical shift changes of the Trp residues in both SH3 domains of p47phox^{SH3A-B}. An alternative explanation could be that two binding pockets for fragments exist in p47phox^{SH3A-B}, one in the SH3A domain and one in the SH3B domain. To investigate this, the eight fragments were injected in a one-step concentration gradient[31,32] at 1 mM over immobilized p47phox^{SH3A-B} allowing a direct comparison of the MW normalized response levels of the eight fragments (Figure 4I). The response levels of **1** and **2** were approximately 2-fold higher compared to **3**−**8**, clearly indicating that **1** and **2** have two binding-sites at p47phox^{SH3A-B}, while **3**−**8** likely have one, in support of the NMR results.

Competition between p22phox and Fragments for Binding to p47phox^{SH3A-B}. The ability of **1**−**8** to compete with p22phox for binding to p47phox^{SH3A-B} was investigated in SPR competition assays. First, this was done in a two-component injection experiment, where p22phox$^{149-168}$ (10 μM) was injected over immobilized p47phox^{SH3A-B} followed by a continuous gradient injection of fragments (up to 1 mM), while the p22phox$^{149-168}$ concentration was kept constant

https://dx.doi.org/10.1021/acs.jmedchem.9b01492
J. Med. Chem. XXXX, XXX, XXX−XXX

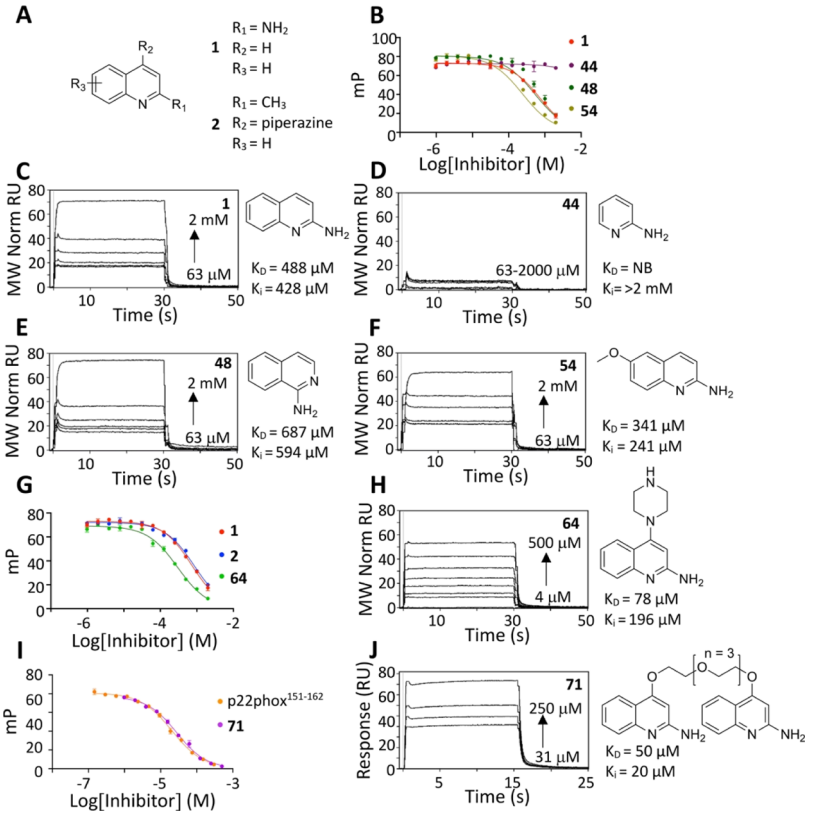

Figure 5. SAR analysis. (A) Fragment hits **1** and **2** share the quinoline scaffold. (B) Fragment hit **1** and analogues **44**, **48** and **54** compete with Cy5-p22phox$^{149-162}$ for binding to p47phox^{SH3A-B} in the FP assay. (C–F) **1**, **44**, **48**, and **54** tested by SPR for binding to immobilized p47phox^{SH3A-B} (5873 RU). **44** did not bind to p47phox^{SH3A-B}, while **48** binds to p47phox^{SH3A-B} with a slightly reduced affinity compared to **1**. **54** binds to p47phox^{SH3A-B} with increased affinity compared to **1**. (G) Merge analogue **64** and parental fragment hits **1** and **2** compete with Cy5-p22phox$^{149-162}$ for binding to p47phox^{SH3A-B} in the FP assay. (H) SPR sensorgrams of **64** injected over immobilized p47phox^{SH3A-B}. (I) Dimeric compound **71** and the p22phox$^{151-161}$ peptide compete with Cy5-p22phox$^{149-162}$ for binding to p47phox^{SH3A-B} in the FP assay. (J) SPR sensorgrams of dimeric compound **71** injected over immobilized p47phox^{SH3A-B}.

(Figure 4J). These experiments were performed directly after the injections, as shown in Figure 4I, whereby the normalized binding levels in Figure 4I,J can be directly compared. The response levels for all eight fragments binding to p47phox^{SH3A-B} was significantly reduced when they were injected with p22phox$^{149-168}$ (Figure 4J), which shows that when p47phox^{SH3A-B} is already binding p22phox$^{149-168}$, the ability of the fragments to bind p47phox^{SH3A-B} is reduced. The second competition assay was performed oppositely by injecting the fragments constantly at 1 mM over immobilized p47phox^{SH3A-B} and subsequently, whilst continuously injecting these, adding p22phox$^{149-168}$ (10 μM) by one-step gradient injection (Supporting Information Figure S10). Comparing the experimental response levels with the expected theoretical response, based on the calculated response if both fragment and p22phox$^{149-168}$ are able to bind simultaneously to p47phox^{SH3A-B}, revealed that only fragments **1** and **2** were able to reduce the total binding level by more than 5% and thus compete with p22phox$^{149-168}$ for binding to p47phox^{SH3A-B} (Supporting Information Table S4). The results from the two SPR competition assays illustrate that the ability for the competition is influenced by the order of injection of the competing components. When injecting p22phox$^{149-168}$ before the fragments were injected, the p47phox^{SH3A-B} exists in a more compact peptide-bound conformation and in this case all fragment hits poorly bind p47phox^{SH3A-B}. In the experiments, where the fragments were continuously injected before p22phox$^{149-168}$, we presume that p47phox^{SH3A-B} exist in a more elongated conformation, and in this case fragments **1** and **2** were able to reduce p22phox$^{149-168}$ binding.

Structure–Activity Relationship Studies of Fragments 1 and 2. Fragment hits **1** and **2**, which share the quinoline scaffold, were selected for structure–activity relationship (SAR) studies (Figure 5A). These fragments were the only hits originating as common FP and TSA screen hits that were validated in all SPR assays. Additionally, **1** and **2** showed chemical shift changes of all five Trp indole NHs of p47phox^{SH3A-B}. These NMR data together with the SAXS and SPR data, suggested binding to two sites at the extended conformation of p47phox^{SH3A-B}, one in the SH3A and one in the SH3B domain. Twenty-one analogues (**9**–**29**) of fragment **2** and 41 analogues (**30**–**70**) of fragment **1** were purchased or synthesized (Scheme 1) and tested by FP and SPR (Tables 2 and 3; Figure 5 shows representative data for analogues with reduced, similar, or improved activity). First, the piperazine ring of **2** (R_2) was substituted with N-substituted piperazines (**9**–**12**), N-heterocyclic rings (**13**–**15**), noncyclic alkyl amines (**16**, **17**), or amino groups (**18**), while R_1 and R_3 were maintained as methyl and hydrogen, respectively. The piperidine and homopiperazine rings turned out to be favorable in R_2 leading to 1.5–2-fold improvement in affinity of **13** and **15** relative to **2**, while most of the N-substituted piperazines (**9**–**12**), morpholine (**14**), noncyclic alkyl amine

https://dx.doi.org/10.1021/acs.jmedchem.9b01492
J. Med. Chem. XXXX, XXX, XXX–XXX

Scheme 1. Synthetic Procedures for Analogues of Fragment Hit 1 and 2[a]

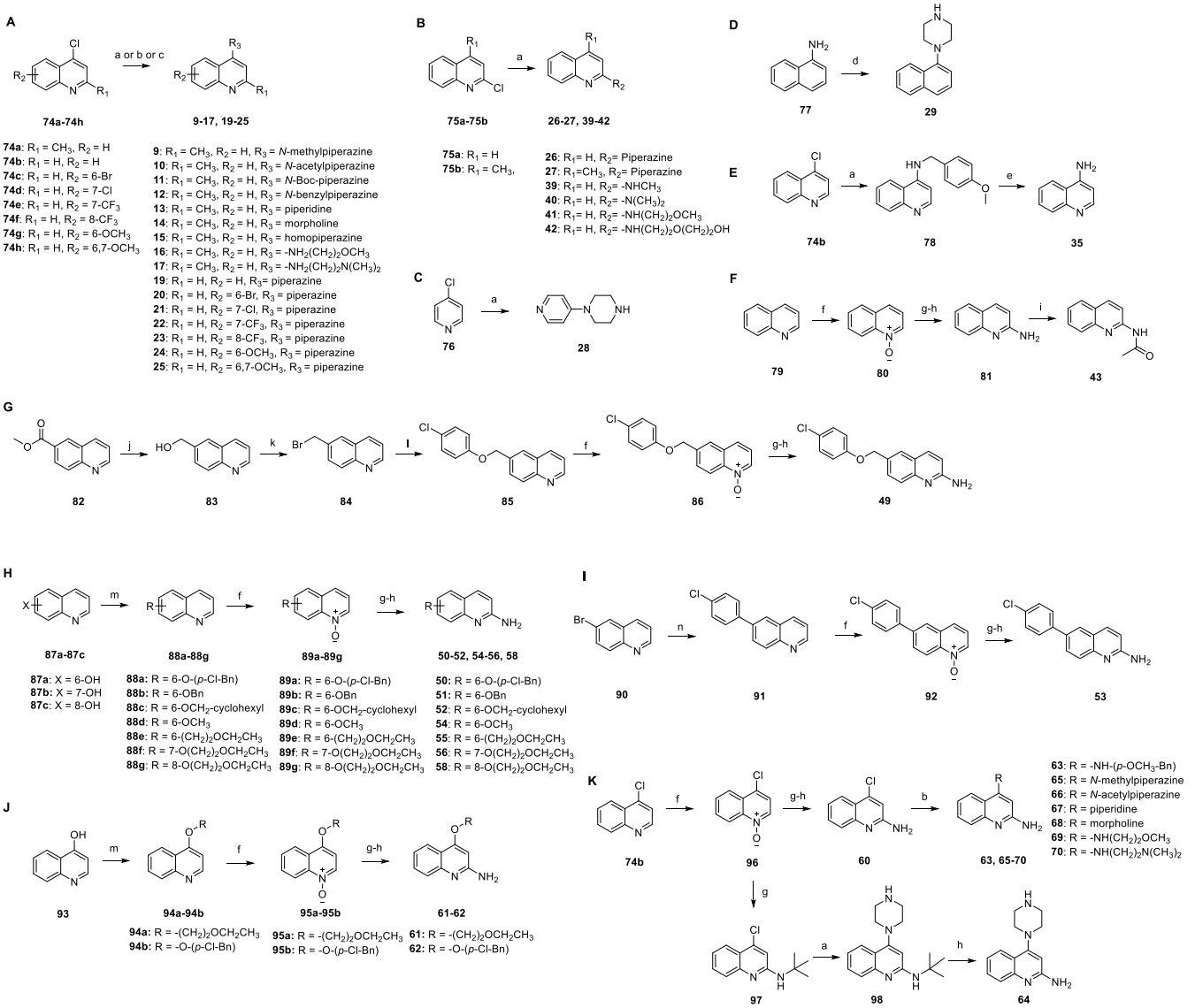

[a]Reagents and conditions: (a) 2-propanol, amine, reflux, 12−24 h; (b) NMP, amine, microwave heating, 200 °C, 15 min; (c) K_2CO_3, homopiperazine, DMF, 120 °C, 24 h; (d) bis(2-chloroethyl)amine hydrochloride, K_2CO_3, diglyme, reflux, 48 h; (e) TFA, rt, overnight; (f) *m*-CPBA, DCM, 0 °C to rt, overnight; (g) *tert*-butylamine, *p*-toluenesulfonic anhydride, trifluorotoluene, DCM, 0 °C to rt, 30 min; (h) TFA, reflux, 3 h; (i) acetyl chloride, triethyl amine, DMAP, DCM, 0 °C, 2h, then excess methylamine, rt, 16 h; (j) $LiAlH_4$, THF, −20 °C, 2 h; (k) PBr_3, DCM, 0 °C to reflux, 2 h; (l) K_2CO_3, 4-chlorophenol, DMF, 80 °C, 16 h; (m) K_2CO_3, organobromide, DMF, 80 °C, 16 h; (n) (4-chlorophenyl)boronic acid, K_2CO_3, $Pd(PPh_3)_4$, dioxane/H_2O, reflux, 2 h; **89e** was commercially available.

(**16**), and amine (**18**) led to reduced affinities compared to **2**. However, the noncyclic alkyl amine as in **17**, containing both a secondary and a tertiary amine like a piperazine, was equipotent to fragment **2**. Next, we found that replacing the methyl group (R_1) of **2** with H gave compound **19** with similar affinity as **2**. We then used this scaffold to explore substitutions of R_3 including halogens (**20**, **21**), electron-withdrawing trifluoromethyl groups (**22**, **23**), and electron-donating methoxy groups (**24**, **25**) on the benzene ring of the quinoline. The 6-Br substituted analogue (**20**) stood out from this series and increased the binding affinity in FP 3-fold compared to **2** or **19**. The remaining compounds gave affinities either similar to **19** (**21**, **22**, **24**, **25**) or lower (**23**). Re-scaffolding of the quinoline ring and the position of piperazine were then investigated. We found that piperazine at position 4 (**2**, **19**) is favored over position 2 (**26**, **27**), as the latter resulted in approximately a two-fold decrease in affinity. When the quinoline ring was replaced with a pyridine scaffold a two-fold increase in affinity was observed by FP for compound **28** relative to (**19**), while the naphthalene analogue (**29**) gave a 2.5-fold reduction in affinity (Table 2).

For **1**, close analogues revealed that the free amino group (R_1) is crucial for activity, as replacements (**30**−**33**), position change (**34**−**38**), or alkylation/acetylation (**39**−**43**) resulted in an almost complete loss of affinity. More dramatic changes of the quinoline scaffold to pyridine, pyrimidine, naphthalene, or benzo[*d*]thiazole also resulted in inactive compounds (**44**−**47**), while the isoquinoline compound (**48**) showed only a 1.5-fold reduction in affinity compared to **1**. Based on this, further modifications were carried out on the conserved 2-amino-

https://dx.doi.org/10.1021/acs.jmedchem.9b01492
J. Med. Chem. XXXX, XXX, XXX−XXX

Table 2. SAR Analysis of Fragment Hit 2 Analogues

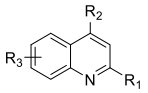

Compds	R_1	R_2	R_3	FP K_i (μM)[a]	SPR K_D (μM)[b]
2	CH_3	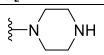	H	606 ± 25	412 ± 130
9	CH_3	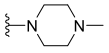	H	> 2000	W
10	CH_3	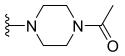	H	815 ± 96	W
11	CH_3	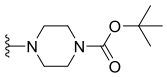	H	> 2000	NB
12	CH_3	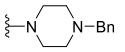	H	1000 ± 480	W
13	CH_3		H	403 ± 20	470
14	CH_3		H	1600 ± 110	597
15	CH_3	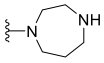	H	271 ± 32	296
16	CH_3	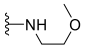	H	1120 ± 23	997
17	CH_3	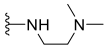	H	722 ± 39	332
18	CH_3	NH_2	H	1070 ± 88	521
19	H		H	697 ± 77	487
20	H		6-Br	231 ± 6.6	NT
21	H		7-Cl	583 ± 24	W
22	H		7-CF_3	894 ± 35	W
23	H		8-CF_3	1540 ± 230	W
24	H		6-OCH_3	466 ± 37	345
25	H		6,7-OCH_3	598 ± 62	318
26		H	H	1410 ± 84	420
27		CH_3	H	1070 ± 130	W
28		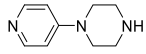		302 ± 20	NB
29		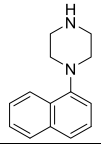		1520 ± 80	366

[a] K_i values are reported as the mean ± SEM ($n \geq 3$). [b] K_D values are reported based on $n = 1$ or $n = 2-3$ (mean ± SEM). NB = no binding (MW norm response max <20% compared to parental fragment hit **2**), W = weaker binding (MW norm response max >20, <50% compared to parental fragment hit **2**), NT = not tested.

quinoline binding core. Noticeably, 6-substituted-2-amino-quinolines have been reported in the literature as small-molecule ligands for Tec SH3 protein domains with 6-[(4-chlorophenoxy)methyl]quinolin-2-amine as the most potent compound showing a K_D of 9 μM by NMR.[33−35] Inspired by this, we investigated various substitutions on the 6-position of the quinoline ring including the mentioned literature compound (**49**). However, in contrast to the published activity against Tec SH3, **49** was not active by either FP or SPR measuring inhibition of the p47phox−p22phox interaction and binding to p47phox, respectively, and it also had poor solubility properties. Small modifications based on **49** were conducted in an attempt to improve affinity, but the resulting compounds (**50**−**53**) were also weak binders with solubility issues like **49**. However, substitutions with methoxy (**54**) or linear alkoxy groups (**55**−**56**) on the 6- and 7-position of **1** resulted in the same or two-fold improved affinities compared to **1**, while substitutions on the 8-position with hydroxy (**57**) or an alkoxy-group (**58**) were not well-tolerated resulting in decreased affinity. Instead, we studied the SAR around the 4-position of **1** (R_2), where it was observed that small substitutions such as OH (**59**) and Cl (**60**) were not favored, while the linear alkoxy group as in (**61**) restored the affinity. Installing the same substitution group as found in the

https://dx.doi.org/10.1021/acs.jmedchem.9b01492
J. Med. Chem. XXXX, XXX, XXX−XXX

Table 3. SAR Analysis of Fragment Hit 1 Analogues

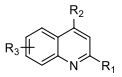

Compds	R_1	R_2	R_3	FP K_i (μM)[a]	SPR K_D (μM)[b]
1	NH_2	H	H	428 ± 23	488 ± 130
30	H	H	H	> 2000	NB
31	CH_3	H	H	> 2000	W
32	OH	H	H	> 2000	NB
33	$-CH_2NH_2$	H	H	> 2000	NB
34	H	H	5-NH_2	> 2000	W
35	H	NH_2	H	1520 ± 160	765
36	H	H	6-NH_2	> 2000	NB
37	H	H	8-NH_2	> 2000	NB
38		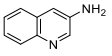		> 2000	W
39		H	H	1370 ± 220	W
40		H	H	1660 ± 140	W
41		H	H	> 2000	NB
42	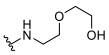	H	H	> 2000	NB
43		H	H	> 2000	NB
44				> 2000	NB
45				> 2000	NB
46		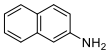		> 2000	NB
47		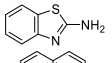		> 2000	NB
48				594 ± 8.7	687
49	NH_2	H	6-CH_2O- 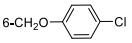	> 2000	NB
50	NH_2	H	6-OCH_2- 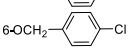	> 2000	NB
51	NH_2	H	6-OCH_2- 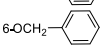	> 2000	W
52	NH_2	H	6-OCH_2- 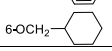	> 2000	W

Compds	R_1	R_2	R_3	FP K_i (μM)[a]	SPR K_D (μM)[b]
53	NH_2	H	6-(*p*-Cl-Ph)	> 2000	NB
54	NH_2	H	6-OCH_3	241 ± 16	341
55	NH_2	H	6-$O(CH_2)_2OCH_2CH_3$	373 ± 14	562 ± 56
56	NH_2	H	7-$O(CH_2)_2OCH_2CH_3$	254 ± 8.5	599 ± 68
57	NH_2	H	8-OH	1380 ± 190	*
58	NH_2	H	8-$O(CH_2)_2OCH_2CH_3$	1250 ± 120	987
59	NH_2	OH	H	> 2000	NB/W
60	NH_2	Cl	H	> 2000	W
61	NH_2	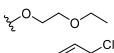	H	512 ± 22	153
62	NH_2	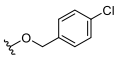	H	> 2000	W
63	NH_2	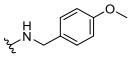	H	243 ± 2.4	NT
64	NH_2		H	196 ± 15	78 ± 39
65	NH_2		H	597 ± 42	643 ± 170
66	NH_2	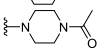	H	475 ± 19	820
67	NH_2		H	186 ± 11	109
68	NH_2		H	435 ± 13	140
69	NH_2		H	658 ± 53	97
70	NH_2		H	592 ± 40	574 ± 4
71		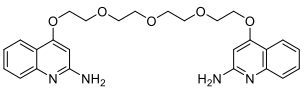		20.0 ± 0.95	50 ± 3
72		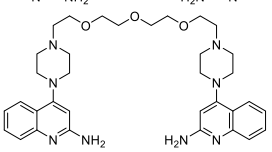		30.0 ± 3.2	177 ± 16
73		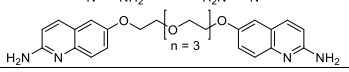		32.7 ± 2.9	*

[a] K_i values are reported as the mean ± SEM ($n \geq 3$). [b] K_D values are reported based on $n = 1$ or $n = 2-3$ (mean ± SEM). NB = no binding (MW norm response max <20% compared to parental fragment hit **1**), W = weaker binding (MW norm response max >20, <50% compared to parental fragment hit **1**), NT = not tested, *ambiguous SPR binding curve.

"literature compound" (**49**), but here in the 4-position, gave the inactive compound **62**, while the substitution of 4-methoxybenzylamine gave compound **63** showing a two-fold improvement in affinity relative to **1**. Considering the importance of the piperazine ring in R_2 of **2** (**2** vs **31**) and the amino group in R_1 of **1** (**1** vs **30**), we expected the merge of the two hits **1** and **2** to show improved affinity, and indeed compound **64** demonstrated 2−3-fold lower K_i values by FP relative to parent fragment hits and also showed enhanced binding by SPR (K_D = 78 μM) (Figure 5G,H and Table 3). We thus elaborated on this merged scaffold with compounds **65**−**70** by modifying or substituting the piperazine ring similar to what we did for the analogues of **2** (Table 3). Interestingly, some of the same trends were seen, as methylation or acetylation of the piperazine (compound **65** and **66**, respectively) reduced the affinity, as did the ring-opening of the piperazine to compound **69** and **70**, while the piperidine compound **67** was equipotent to **64**. In this case, the morpholine substitution resulted in only a two-fold reduction in affinity (**68** vs **64**) (Table 3).

Overall, several analogues showed improved affinities relative to parent fragment hit **1** and **2**, however, to a rather modest extent with a 2-3-fold decrease in K_i values for compounds **13**, **15**, **20**, **28**, **54**, **56**, **63**, **64**, and **67**. Thus, it seemed that to obtain more dramatic improvements in inhibitory activity and binding affinity, more unconventional means were required. Hence, considering that our SPR and NMR data (Figure 4 and Supporting Information Figure S8) suggest that **1** and **2** bind to both SH3 domains of p47phox, we envisioned that connecting these fragments by a flexible linker which is able to span both SH3 domains affording a homodimeric compound would lead to more significant affinity improvements, as has been reported for other protein targets.[36,37] Based on our SAR study, the 4-, 6-, and 7-positions could provide suitable attachment points for linkers. Thus, the three dimeric compounds **71**−**73** were designed and synthesized (Scheme 2). Encouragingly, the three dimers gave a 13−30-fold improved affinity by FP compared to the monomeric parent fragment hits **1** and **2** (Table 3). Among the three dimeric compounds, **71** was the most potent dimer with

https://dx.doi.org/10.1021/acs.jmedchem.9b01492
J. Med. Chem. XXXX, XXX, XXX−XXX

Scheme 2. Synthesis of Dimeric p47phox−p22phox Inhibitors Compound 71, 72, and 73[a]

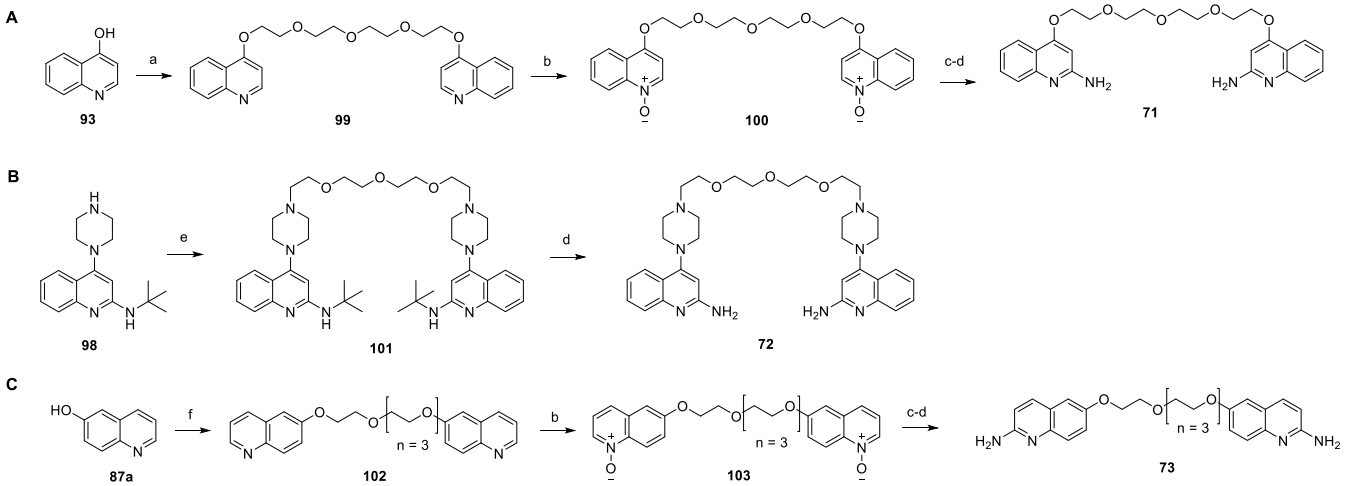

[a]Reagents and conditions: (a) Cs_2CO_3, 1,11-dibromo-3,6,9-trioxaundecane, DMF, 80 °C, 2 h; (b) *m*-CPBA, DCM, 0 °C to rt, overnight; (c) *tert*-butylamine, *p*-toluenesulfonic anhydride, trifluorotoluene, DCM, 0 °C to rt, 30 min; (d) TFA, reflux, 3 h; (e) tetraethylene glycol, K_2CO_3, rt, overnight; (f) tetraethylene glycol, PPh_3, DIAD, THF, rt, 72 h.

a K_i of 20 μM in FP, which is similar to the p22phox$^{151-162}$ peptide (K_i = 17 μM at 2% DMSO), and with confirmed binding in SPR (K_D = 50 μM) (Figure 5I,J). As a control experiment for potential aggregation artifacts, **71−73** were tested by FP in the presence of 0.01% Triton-X and showed the same affinities as without the presence of Triton-X within the experimental error (Supporting Information Figure S11).

Binding Model. The competition assays show that fragments **1** and **2** could reduce binding of p22phox to p47phox, and SPR, NMR, and SAXS data suggest that **1** and **2** bind to both SH3 domains of the extended conformation of p47phox. We propose that inhibition could be either because of the fragments sterically preventing p22phox$^{149-168}$ binding or because the fragments stabilize the extended conformation of p47phox^{SH3A-B} and prevent the formation of the compact conformation required for creating the binding pocket to p22phox$^{149-168}$ (Figure 6A). Based on this, we designed the dimeric compounds **71−73**, and the improved affinity seen for these supports the proposed binding mode of the original fragments. Likewise, these data support that the dimeric compounds occupy both SH3 domains in p47phox^{SH3A-B} in a binding mode that is likely facilitated by the interdomain flexibility of p47phox^{SH3A-B} and the conformational flexibility of the polyethylene glycol (PEG)-linker of the compounds (Figure 6B). Interestingly, NMR binding studies of 2-aminoquinoline with the mouse Tec kinase SH3 single domain indicated that the two residues Trp^{215} and Asp^{196} in the Tec kinase SH3 sequence are important for binding.[34] Similar residues are found in p47phox^{SH3A-B}, as Trp^{215} is conserved for SH3A (Trp^{193}) and SH3B (Trp^{263}), while Asp^{196} is conservatively exchanged to a glutamic acid in p47phox SH3A (Glu^{174}) and SH3B (Glu^{254}) (Supporting Information Figure S12). Combined with our data, this homology further supports that fragments (**1** and **2**) and dimeric compounds (e.g., **71**) bind to p47phox^{SH3A-B} at sites composed of key amino acids at both SH3A (Glu^{174}, Trp^{193}) and SH3B (Glu^{254}, Trp^{263}) (Figure 6).

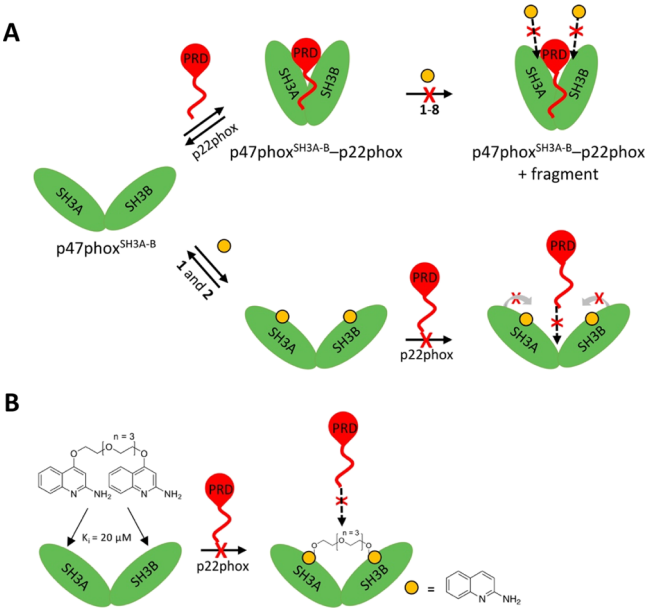

Figure 6. Model of fragments and dimeric compounds binding to p47phox. (A) When blocking the tandem SH3 domains of p47phox^{SH3A-B} with the p22phox-derived peptide p22phox$^{149-168}$ the fragments' ability to bind p47phox^{SH3A-B} was significantly reduced. Fragment hits **1** and **2** were found to bind one site in SH3A and another site in SH3B of the extended conformation of p47phox^{SH3A-B}. Binding of **1** and **2** to p47phox^{SH3A-B} reduced p22phox$^{149-168}$ binding either because of steric hindrance or by stabilizing the extended conformation of p47phox^{SH3A-B}. (B) Proposed binding mode of dimeric compounds to p47phox^{SH3A-B}.

CONCLUSIONS

Reduction of NADPH oxidase 2 activity by inhibiting the p47phox−p22phox interaction is a potential strategy for therapeutic intervention of oxidative stress. To date, ebselen is the only small-molecule shown able to bind p47phox and prevent the interaction with p22phox.[13]

Here, we demonstrate that ebselen covalently reacts with Cys^{196} of p47phox^{SH3A-B}, leading to destabilization and aggregation of the protein; a mechanism of action that is not

https://dx.doi.org/10.1021/acs.jmedchem.9b01492
J. Med. Chem. XXXX, XXX, XXX−XXX

promising for further drug development, nor warrant its use as a chemical probe. Instead, we identified eight fragment hits (**1**–**8**)—by screening 2500 fragments using FP and TSA followed by hit validation by SPR—which bind p47phox^{SH3A-B} and serve as scaffolds for developing reversible and drug-like small-molecule inhibitors. The quinolone fragment hits **1** and **2** were the only common hits across all assays and were able to reduce the binding of p22phox to p47phox^{SH3A-B}. Binding as well as structural NMR data suggested that they interact with two sites on p47phox^{SH3A-B}, presumably at the SH3A and SH3B domain, and interestingly, SAXS studies suggested that **1** and **2** bind p47phox^{SH3A-B} when this is in an extended conformation instead of the compact conformation seen when p22phox peptide binds.

Sixty-five analogues of **1** and **2** were designed and synthesized. Several smaller modifications gave affinity improvements of 2–3-fold compared to parent fragment hits. However, the biggest improvement in affinity was obtained by connecting fragments **1** and **2** by a PEG-based linker, affording the three homodimeric compounds **71**–**73** with 13–30-fold higher affinities than **1** and **2**, and the best dimer (**71**) being equipotent to the p22phox$^{151-162}$ peptide (K_i = 20 μM). This dimeric design was incited by our SPR, SAXS, and NMR data suggesting that **1** and **2** bind to both SH3 domains of p47phox, and the improved affinity seen for the dimeric compounds support the proposed binding mode of the fragments.

By FBDD, we have developed the first nonpeptide reversible inhibitors of the p47phox–p22phox protein–protein interaction. The best compounds are dimeric with affinities similar to the shorter p22phox-derived peptide p22phox$^{151-162}$. However, further optimization is needed to reach affinities relevant for more advanced biological studies, such as cell-free or cell-based ROS detection assays and cell-based oxygen consumption measurements.[14,38] Our SAR study and proposed binding model based on biophysical and structural data provide encouraging results and guidance for future directions. Hopefully these data can facilitate the development of chemical probes suitable for studying the therapeutic relevance of NADPH oxidase 2 inhibition.

EXPERIMENTAL SECTION

Chemistry. *General Procedures.* All commercially available solvents and reagents were purchased and used without further purification. Room temperature refers to 20–22 °C. Normal-phase chromatography was executed on a TELEDYNE ISCO apparatus (CombiFlash Rf), using silica gel as the stationary phase and mixtures of ethyl acetate and heptane or dichloromethane (DCM) and methanol (MeOH) as eluents. Preparative reverse-phase (RP) chromatography was performed on an Agilent 1200 series high-performance liquid chromatography (HPLC) system using a C18 reverse column (ZORBAX 300SB-C18 PrepHT, 21.2 × 250 mm, 7 μm) with a linear gradient of the binary solvent system of H_2O/CH_3CN/trifluoroacetic acid (TFA) (A: 95/5/0.1, and B: 5/95/0.1) with a flow rate of 20 mL/min. Microwave heating was performed on a Biotage Initiator 2.5. NMR spectra were recorded on a 600 MHz Bruker AVANCE III HD instrument equipped with a cryogenically cooled 5 mm dual probe or 400 MHz Bruker AVANCE II instrument equipped with a 5 mm broadband probe. Deuterated DMSO (DMSO-d_6) or deuterated chloroform ($CDCl_3$) were used as solvents. Chemical shifts for ^{1}H and ^{13}C spectra were reported in parts per million (ppm) and coupling constants were reported in Hertz. LC–MS analyses carried out using an Agilent 6410 Triple Quadrupole mass spectrometer instrument with electron spray ionization (ESI) coupled to an Agilent 1200 HPLC system (ESI-LC/MS) with a C18 reverse phase column (Zorbax Eclipse XBD-C18, 4.6 mm × 50 mm), autosampler and diode array detector using a linear gradient of the binary solvent system of H_2O/CH_3CN/formic acid (A: 95/5/0.1, and B: 5/95/0.043). Also, evaporative light-scattering traces were obtained with a Sedere Sedex 85 light scattering detector. The LC–MS method for all the target compounds is as follows: ESI, 0% B to 100% B, run time = 5 min, flow rate = 1 mL/min. Compounds **18**, **30**–**34**, **36**–**38**, **44**–**48**, **57** and **59** were purchased and showed ≥95% purity by NMR (^{1}H, ^{13}C) and LC–MS (UV). All other final compounds were synthesized and showed ≥95% purity, as determined by NMR (^{1}H, ^{13}C, ^{1}H–^{1}H COSY, ^{1}H–^{13}C HSQC) and LC–MS (UV).

Peptides. TAMRA-labeled peptide p22phox$^{151-162}$ (5(6)TAMRA-PPTNPPPRPPAE-NH_2) and unlabeled peptides—p22phox$^{151-162}$ (Ac-PPTNPPPRPPAE-NH_2), p22phox$^{149-168}$ (Ac-KQPPSNPPPRPPAEARKKPS-NH_2), and p22phox$^{149-162}$ (Ac-CKQPPSNPPPRPPAE-NH_2)—were purchased from Biomatik. The Cy5-labeled peptide p22phox$^{149-162}$ with sequence Ac-C(Cy5)-KQPPSNPPPRPPAE-NH_2 was generated by mixing unlabeled peptide Ac-CKQPPSNPPPRPPAE-NH_2 (2.24 mg) dissolved in 1.7 mL of buffer (50 mM 4-(2-hydroxyethyl)-1-piperazineethanesulfonic acid (Hepes), 150 mM NaCl, pH 7.4) with sulfo-Cy5-maleimide (1.14 mg; Lumiprobe) dissolved in 40 μL of DMSO followed by incubation for 2 h, HPLC purification, and lyophilization. All peptides were analyzed by LC–MS and showed ≥95% purity.

General Procedure A for the Synthesis of 9–14, 17, 19, 21–23, 25–28, 39–42, and 78. A mixture of properly substituted 4-chloroquinoline or 2-chloroquinoline (1 equiv) and amines (2 equiv) in isopropyl alcohol (3 mL) was refluxed for 12–24 h. The solvent was evaporated in vacuo, and the resulting residue was purified by silica gel column chromatography (**9**–**14**, **19**, **21**–**23**, **25**–**28**, **39**–**42**, **78**) or RP-HPLC (**17**) to obtain the desired product.

General Procedure B for the Synthesis of 16, 20, 24, 63, and 65–70. A mixture of properly substituted 4-chloroquinoline or 4-chloroquinoline-2-amine (1 equiv) and amines (2 equiv) in NMP (1 mL) was heated at 200 °C for 15 min in a microwave reactor. After cooling to room temperature, the reaction mixture was diluted with water and extracted three times with ethyl acetate. The combined organic layers were washed with brine, dried over Na_2SO_4, filtered, and concentrated. The residue was purified by silica gel column chromatography (**20**, **63**, and **65**–**69**) or RP-HPLC (**16**, **24**, and **70**) to afford the desired product.

General Procedure C for the Synthesis of 80, 86, 89a–89g, 92, 95a–95b, 96, 100, and 103. To a solution of properly substituted quinoline (1 equiv) in DCM (15 mL) at 0 °C was added *m*-CPBA (1.5 equiv or 3 equiv). The reaction mixture was allowed to warm to room temperature and stirred overnight. The reaction was quenched with 1 M NaOH until pH = 10. The aqueous layer was extracted with DCM three times and the combined organic extracts were dried over Na_2SO_4, filtered, and concentrated under reduced pressure. The crude product was used without further purification, unless otherwise stated.

General Procedure D for the Synthesis of 49–56, 58, 60–62, 71, 73, and 81. The properly substituted quinoline 1-oxide (1 equiv) was diluted in 2:1 trifluorotoluene/DCM and cooled to 0 °C. *tert*-Butylamine (5 equiv or 10 equiv) was added, followed by *p*-toluenesulfonic anhydride (2 equiv or 4 equiv) in small portions. After 30 min, the suspension was concentrated. TFA (5 mL) was added, and the mixture was heated to reflux for 3 h. The mixture was concentrated and neutralized with 1 M NaOH until the pH was ∼12. The suspension was extracted with DCM three times. The combined organic layers were dried over Na_2SO_4, filtered, and concentrated under reduced pressure. The crude was purified by silica gel column chromatography to yield the desired product.

General Procedure E for the Synthesis of 88a–88g and 94a–94b. To a suspension of K_2CO_3 (1.5 equiv) and 4-, 6-, 7-, or 8-hydroxyquinoline (1 equiv) in dimethylformamide (DMF) (8 mL) was added various bromide (1.1 equiv). The mixture was stirred at 80 °C for 16 h. The reaction was quenched with water, extracted with ethyl acetate three times, washed with 1 M NaOH, brine, and dried over Na_2SO_4, filtered, and concentrated under reduced pressure. The

https://dx.doi.org/10.1021/acs.jmedchem.9b01492
J. Med. Chem. XXXX, XXX, XXX–XXX

crude was purified by silica gel column chromatography to obtain the desired product.

*2-Methyl-4-(4-methylpiperazin-1-yl)quinoline (**9**).* The reaction was carried out following the general procedure A, using **74a** (0.20 g, 1.13 mmol) and 1-methylpiperazine (0.23 g, 2.26 mmol). Yellow oil (0.20 g, 73%). ^{1}H NMR (400 MHz, DMSO-d_6): δ 7.84 (dd, J = 8.4, 1.4 Hz, 1H), 7.74 (dd, J = 8.5, 1.2 Hz, 1H), 7.53 (ddd, J = 8.3, 6.8, 1.4 Hz, 1H), 7.36 (ddd, J = 8.2, 6.8, 1.3 Hz, 1H), 3.10−3.01 (m, 4H), 2.47 (s, 3H), 2.43−2.38 (m, 4H), 2.19 (s, 3H). ^{13}C NMR (101 MHz, DMSO): δ 158.97, 156.18, 148.72, 128.85, 128.79, 124.38, 123.45, 121.18, 109.35, 54.58 (2C), 51.59 (2C), 45.70, 25.06. LC−MS: $[M + H]^+$, 242.2, t_R = 0.53 min.

*1-(4-(2-Methylquinolin-4-yl)piperazin-1-yl)ethan-1-one (**10**).* The reaction was carried out following the general procedure A, using **74a** (0.20 g, 1.13 mmol) and 1-acetylpiperazine (0.29 g, 2.26 mmol). White crystalline (60 mg, 20%). ^{1}H NMR (400 MHz, DMSO-d_6): δ 8.01 (d, J = 7.5 Hz, 1H), 7.86 (d, J = 7.6 Hz, 1H), 7.65 (ddd, J = 8.3, 6.8, 1.4 Hz, 1H), 7.53−7.44 (m, 1H), 6.89 (s, 1H), 3.72 (d, J = 4.9 Hz, 6H), 3.19−3.13 (m, 4H), 3.12−3.06 (m, 4H), 2.58 (s, 3H), 2.07 (s, 3H). ^{13}C NMR (101 MHz, DMSO): δ 168.43, 159.04, 155.91, 148.73, 128.95, 128.88, 124.63, 123.44, 121.16, 109.73, 51.91, 51.62, 45.69, 40.86, 25.08, 21.25. LC−MS: $[M + H]^+$, 270.3, t_R = 1.47 min.

*tert-Butyl 4-(2-Methylquinolin-4-yl)piperazine-1-carboxylate (**11**).* The reaction was carried out following the general procedure A, using **74a** (0.20 g, 1.13 mmol) and 1-Boc-piperazine (0.42 g, 2.26 mmol). White solid (0.18 g, 49%). ^{1}H NMR (400 MHz, DMSO-d_6): δ 7.98 (dd, J = 8.4, 1.4 Hz, 1H), 7.85 (dd, J = 8.5, 1.2 Hz, 1H), 7.64 (ddd, J = 8.4, 6.8, 1.4 Hz, 1H), 7.47 (ddd, J = 8.2, 6.8, 1.3 Hz, 1H), 6.90 (s, 1H), 3.60 (d, J = 9.9 Hz, 2H), 3.13−3.06 (m, 4H), 2.57 (s, 3H), 1.44 (s, 9H). ^{13}C NMR (101 MHz, DMSO): δ 159.02, 156.01, 153.90, 148.72, 128.91, 128.86, 124.59, 123.42, 121.18, 109.75, 79.06, 51.61 (2C), 43.57 (2C), 28.05 (3C), 25.07. LC−MS: $[M + H]^+$, 328.3, t_R = 2.17 min.

*4-(4-Benzylpiperazin-1-yl)-2-methylquinoline (**12**).* The reaction was carried out following the general procedure A, using **74a** (0.20 g, 1.13 mmol) and 1-benzylpiperazine (0.40 g, 2.25 mmol). Golden brown oil (0.14 g, 39% yield). ^{1}H NMR (400 MHz, DMSO-d_6): δ 7.93 (dd, J = 8.4, 1.4 Hz, 1H), 7.83 (dd, J = 8.5, 1.2 Hz, 1H), 7.62 (ddd, J = 8.3, 6.8, 1.4 Hz, 1H), 7.45 (ddd, J = 8.3, 6.8, 1.3 Hz, 1H), 7.39−7.32 (m, 4H), 7.31−7.24 (m, 1H), 6.87 (s, 1H), 3.60 (s, 2H), 3.16 (t, J = 4.7 Hz, 4H), 2.66 (t, J = 4.7 Hz, 4H), 2.56 (s, 3H). ^{13}C NMR (101 MHz, DMSO): δ 158.98, 156.17, 148.71, 137.97, 128.95 (2C), 128.84, 128.80 (2C), 128.20, 127.00, 124.41, 123.47, 121.19, 109.35, 62.03, 52.52, 51.74, 25.08. LC−MS: $[M + H]^+$, 214.1, t_R = 1.01 min.

*2-Methyl-4-(piperidin-1-yl)quinoline (**13**).* The reaction was carried out following the general procedure A, using **74a** (0.20 g, 1.13 mmol) and piperidine (0.19 g, 2.25 mmol). White crystalline (20 mg, 7.8% yield). ^{1}H NMR (400 MHz, chloroform-d): δ 7.97 (dd, J = 8.5, 1.2 Hz, 1H), 7.94 (dd, J = 8.5, 1.5 Hz, 1H), 7.59 (ddd, J = 8.4, 6.8, 1.5 Hz, 1H), 7.39 (ddd, J = 8.2, 6.8, 1.3 Hz, 1H), 6.69 (s, 1H), 3.24−3.12 (m, 4H), 2.66 (s, 3H), 1.84 (dq, J = 11.1, 5.3 Hz, 4H), 1.68 (qd, J = 5.9, 5.4, 3.8 Hz, 2H). ^{13}C NMR (101 MHz, $CDCl_3$): δ 159.27, 158.30, 149.03, 129.12, 128.89, 124.42, 123.83, 122.13, 109.24, 53.71 (2C), 26.24 (2C), 25.53, 24.60. LC−MS: $[M + H]^+$, 227.2, t_R = 1.90 min.

*4-(2-Methylquinolin-4-yl)morpholine (**14**).* The reaction was carried out following the general procedure A, using **74a** (0.20 g, 1.13 mmol) and morpholine (0.20 g, 2.25 mmol). Pale yellow solid (90 mg, 35%). ^{1}H NMR (400 MHz, DMSO-d_6): δ 7.99 (dd, J = 8.4, 1.4 Hz, 1H), 7.85 (dd, J = 8.4, 1.2 Hz, 1H), 7.64 (ddd, J = 8.4, 6.9, 1.5 Hz, 1H), 7.46 (ddd, J = 8.2, 6.8, 1.3 Hz, 1H), 6.89 (s, 1H), 3.95−3.80 (m, 4H), 3.22−3.07 (m, 4H), 2.58 (s, 3H). ^{13}C NMR (101 MHz, DMSO): δ 159.05, 156.05, 148.75, 128.88 (2C), 124.50, 123.47, 121.07, 109.35, 66.13 (2C), 52.21 (2C), 25.08. LC−MS: $[M + H]^+$, 229.2, t_R = 1.59 min.

*4-(1,4-Diazepan-1-yl)-2-methylquinoline (**15**).* A mixture of **74a** (0.20 g, 1.13 mmol), homopiperazine (0.23 g, 2.26 mmol) and K_2CO_3 (0.31 g, 2.26 mmol) in DMSO (2 mL) was heated at 120 °C for 24 h. The reaction mixture was diluted with water and extracted with ethyl acetate three times. The combined organic phrases were dried over Na_2SO_4, filtered, and concentrated. The crude product was purified by silica gel column chromatography (eluting with a gradient of 0−10% MeOH in DCM) to obtain the desired product. Pale yellow crystalline (20 mg, 7.3%). ^{1}H NMR (600 MHz, chloroform-d): δ 7.96 (dd, J = 8.5, 1.4 Hz, 1H), 7.92 (dd, J = 8.4, 1.3 Hz, 1H), 7.56 (ddd, J = 8.3, 6.8, 1.4 Hz, 1H), 7.34 (ddd, J = 8.3, 6.8, 1.3 Hz, 1H), 6.69 (s, 1H), 3.53−3.50 (m, 2H), 3.49−3.47 (m, 2H), 3.13−3.10 (m, 2H), 3.10−3.07 (m, 2H), 2.62 (s, 3H), 2.58 (s, 1H), 2.00 (p, J = 5.8 Hz, 2H). ^{13}C NMR (151 MHz, $CDCl_3$): δ 158.95, 158.10, 149.63, 129.06, 128.91, 124.16, 123.89, 121.89, 108.85, 57.39, 54.18, 49.33, 48.40, 30.85, 25.60. LC−MS: $[M + H]^+$, 242.2, t_R = 0.55 min.

*N-(2-Methoxyethyl)-2-methylquinolin-4-amine Monotrifluoroacetate (**16**).* The reaction was carried out following the general procedure B, using **74a** (0.20 g, 1.13 mmol) and 2-methoxyethanamine (0.17 g, 2.26 mmol). Pale yellow solid (0.13 g, 35%). ^{1}H NMR (400 MHz, DMSO-d_6): δ 13.61 (s, 1H), 9.07 (t, J = 5.6 Hz, 1H), 8.47 (dd, J = 8.6, 1.3 Hz, 1H), 7.92 (ddd, J = 8.3, 6.9, 1.2 Hz, 1H), 7.84 (dd, J = 8.6, 1.3 Hz, 1H), 7.66 (ddd, J = 8.3, 6.9, 1.3 Hz, 1H), 6.86 (s, 1H), 3.70 (dd, J = 6.1, 4.6 Hz, 2H), 3.64 (td, J = 5.2, 4.8, 1.2 Hz, 2H), 2.64 (s, 3H). ^{13}C NMR (101 MHz, DMSO): δ 155.28, 153.82, 137.81, 133.32, 126.08, 122.88, 119.55, 115.58, 98.52, 69.38, 58.17, 42.82, 19.95. LC−MS: $[M + H]^+$, 217.1, t_R = 1.61 min.

*N^1,N^1-Dimethyl-N^2-(2-methylquinolin-4-yl)ethane-1,2-diamine Ditrifluoroacetate (**17**).* The reaction was carried out following the general procedure A, using **74a** (0.20 g, 1.13 mmol) and *N*,*N*-dimethylethylenediamine (0.20 g, 2.26 mmol). White to beige solid (80 mg, 15%). ^{1}H NMR (400 MHz, DMSO-d_6): δ 14.28 (s, 1H), 8.97 (s, 2H), 8.33 (d, J = 8.6 Hz, 1H), 7.98−7.88 (m, 2H), 7.63 (dt, J = 8.5, 4.1 Hz, 1H), 7.06 (s, 1H), 3.99 (t, J = 6.7 Hz, 2H), 3.46 (s, 3H), 3.40 (s, 3H), 2.74−2.59 (m, 7H). ^{13}C NMR (101 MHz, DMSO): δ 159.81, 158.53, 158.21, 153.07, 139.58, 133.11, 127.03, 125.26, 119.74, 118.56, 117.56, 115.59, 104.83, 50.61, 44.66, 43.07, 32.78, 19.81. LC−MS: $[M + H]^+$, 230.2, t_R = 0.74 min.

*4-(Piperazin-1-yl)quinoline (**19**).* The reaction was carried out following the general procedure A, using **74b** (0.20 g, 1.22 mmol) and piperazine (0.21 g, 2.44 mmol). Oily yellow solid (0.11 g, 42%). ^{1}H NMR (400 MHz, DMSO-d_6): δ 8.67 (d, J = 5.0 Hz, 1H), 8.02 (dd, J = 8.4, 1.5 Hz, 1H), 7.93 (dd, J = 8.4, 1.3 Hz, 1H), 7.68 (ddd, J = 8.4, 6.8, 1.5 Hz, 1H), 7.53 (ddd, J = 8.2, 6.7, 1.3 Hz, 1H), 6.95 (d, J = 4.9 Hz, 1H), 3.12−3.05 (m, 4H), 2.97 (dd, J = 6.0, 3.5 Hz, 4H). ^{13}C NMR (101 MHz, DMSO): δ 156.70, 150.84, 149.11, 129.54, 128.86, 125.15, 123.80, 122.78, 108.79, 53.19 (2C), 45.56 (2C). LC−MS: $[M + H]^+$, 214.1, t_R = 0.47 min.

*6-Bromo-4-(piperazin-1-yl)quinoline (**20**).* The reaction was carried out following the general procedure B, using **74c** (0.10 g, 0.41 mmol) and piperazine (0.07 g, 0.82 mmol). Pale yellow sticky solid (69 mg, 59%). ^{1}H NMR (400 MHz, DMSO-d_6): δ 8.71 (d, J = 5.0 Hz, 1H), 8.10 (d, J = 2.3 Hz, 1H), 7.89 (d, J = 8.9 Hz, 1H), 7.81 (dd, J = 9.0, 2.2 Hz, 1H), 7.02 (d, J = 5.0 Hz, 1H), 3.07 (dd, J = 6.2, 3.2 Hz, 4H), 2.97 (dd, J = 6.1, 3.4 Hz, 4H). ^{13}C NMR (101 MHz, DMSO): δ 155.93, 151.50, 147.73, 132.03, 131.91, 125.73, 124.25, 118.34, 109.92, 53.16 (2C), 45.47 (2C). LC−MS: $[M + H]^+$, 292.1/294.0 (Br), t_R = 0.66 min.

*7-Chloro-4-(piperazin-1-yl)quinoline (**21**).* The reaction was carried out following the general procedure A, using **74d** (0.20 g, 1.01 mmol) and piperazine (0.17 g, 2.02 mmol). Pale yellow solid (51 mg, 20%). ^{1}H NMR (600 MHz, DMSO-d_6): δ 8.69 (d, J = 5.0 Hz, 1H), 8.02 (d, J = 9.0 Hz, 1H), 7.97 (d, J = 2.2 Hz, 1H), 7.55 (dd, J = 9.0, 2.3 Hz, 1H), 6.98 (d, J = 5.0 Hz, 1H), 3.11−3.07 (m, 4H), 2.96 (dd, J = 5.9, 3.7 Hz, 4H), 2.39 (s, 1H). ^{13}C NMR (151 MHz, DMSO): δ 156.89, 152.19, 149.68, 133.46, 128.03, 126.11, 125.59, 121.42, 109.24, 53.21 (2C), 45.51 (2C). LC−MS: $[M + H]^+$, 248.1/250.1 (Cl), t_R = 0.68 min.

*4-(Piperazin-1-yl)-7-(trifluoromethyl)quinoline (**22**).* The reaction was carried out following the general procedure A, using **74e** (0.20 g, 0.86 mmol) and piperazine (0.15 g, 1.72 mmol). White solid (0.15 g, 62%). ^{1}H NMR (400 MHz, DMSO-d_6): δ 8.80 (d, J = 5.0 Hz, 1H), 8.29−8.19 (m, 2H), 7.78 (dd, J = 8.8, 2.0 Hz, 1H), 7.10 (d, J = 5.0

https://dx.doi.org/10.1021/acs.jmedchem.9b01492
J. Med. Chem. XXXX, XXX, XXX−XXX

Hz, 1H), 3.17−3.09 (m, 4H), 3.02−2.94 (m, 4H). ^{13}C NMR (101 MHz, DMSO-d_6): δ 156.67, 152.57, 148.08, 129.09 (q, J_{CF} = 32.0 Hz), 126.93 (q, J_{CF} = 4.4 Hz), 126.06, 124.79, 124.03 (q, J_{CF} = 272.4 Hz), 120.26 (q, J_{CF} = 3.3 Hz), 110.54, 53.15 (2C), 45.46 (2C). LC−MS: $[M + H]^+$, 282.2, t_R = 1.28 min.

*4-(Piperazin-1-yl)-8-(trifluoromethyl)quinoline (**23**).* The reaction was carried out following the general procedure A, using **74f** (0.20 g, 0.86 mmol) and piperazine (0.15 g, 1.72 mmol). White solid (0.19 g, 79%). ^{1}H NMR (400 MHz, DMSO-d_6): δ 8.79 (d, J = 5.0 Hz, 1H), 8.31 (dd, J = 8.6, 1.4 Hz, 1H), 8.11 (dd, J = 7.4, 1.4 Hz, 1H), 7.65 (t, J = 7.9 Hz, 1H), 7.09 (d, J = 5.1 Hz, 1H), 3.17−3.07 (m, 4H), 2.98 (dd, J = 6.1, 3.4 Hz, 4H). ^{13}C NMR (101 MHz, DMSO-d_6): δ 157.15, 151.65, 145.39, 129.02, 127.71 (q, J_{CF} = 5.7 Hz), 126.41 (q, J_{CF} = 28.6 Hz), 124.28 (q, J_{CF} = 273.0 Hz), 123.97, 123.34, 109.74, 53.31 (2C), 45.45 (2C). LC−MS: $[M + H]^+$, 282.2, t_R = 1.63 min.

*6-Methoxy-4-(piperazin-1-yl)quinoline Monotrifluoroacetate (**24**).* The reaction was carried out following the general procedure B, using **74g** (0.10 g, 0.52 mmol) and piperazine (0.09 g, 1.03 mmol). White solid (59 mg, 32%). ^{1}H NMR (400 MHz, DMSO-d_6): δ 9.43 (s, 2H), 8.76 (d, J = 6.3 Hz, 1H), 8.05 (d, J = 9.3 Hz, 1H), 7.66 (dd, J = 9.2, 2.6 Hz, 1H), 7.39−7.24 (m, 2H), 3.99 (s, 3H), 3.85−3.68 (m, 4H), 3.45 (d, J = 5.0 Hz, 4H). ^{13}C NMR (101 MHz, DMSO): δ 159.06, 157.50, 142.29, 136.22, 124.74, 124.11, 121.83, 108.12, 104.09, 55.88, 48.13 (2C), 42.38 (2C). 244.1, LC−MS: $[M + H]^+$, 244.1, t_R = 0.79 min.

*6,7-Dimethoxy-4-(piperazin-1-yl)quinoline (**25**).* The reaction was carried out following the general procedure A, using **74h** (0.1 g, 0.45 mmol) and piperazine (0.08 g, 0.9 mmol). White solid (78 mg, 63%).^{1}H NMR (400 MHz, DMSO-d_6): δ 8.49 (d, J = 5.0 Hz, 1H), 7.30 (s, 1H), 7.21 (s, 1H), 6.84 (d, J = 5.0 Hz, 1H), 3.99−3.85 (m, 6H), 3.09−3.01 (m, 4H), 3.01−2.91 (m, 4H). ^{13}C NMR (101 MHz, DMSO): δ 155.44, 151.46, 148.53, 148.30, 146.00, 117.58, 108.43, 107.78, 101.74, 55.53, 55.31, 52.88 (2C), 45.62 (2C). LC−MS: $[M + H]^+$, 274.1, t_R = 0.85 min.

*2-(Piperazin-1-yl)quinoline (**26**).* The reaction was carried out following the general procedure A, using **75a** (0.20 g, 1.22 mmol) and piperazine (0.21 g, 2.44 mmol). White solid (23 mg, 8.8%). ^{1}H NMR (400 MHz, DMSO-d_6): δ 8.00 (d, J = 9.2 Hz, 1H), 7.68 (dd, J = 7.9, 1.4 Hz, 1H), 7.57−7.47 (m, 2H), 7.24−7.15 (m, 2H), 3.67−3.56 (m, 4H), 2.85−2.76 (m, 4H), 2.46−2.36 (m, 1H). ^{13}C NMR (101 MHz, DMSO): δ 157.30, 147.30, 137.16, 129.27, 127.30, 125.94, 122.63, 121.81, 110.01, 45.79 (2C), 45.61 (2C). LC−MS: $[M + H]^+$, 318.2, t_R = 1.49 min.

*4-Methyl-2-(piperazin-1-yl)quinoline (**27**).* The reaction was carried out following the general procedure A, using **75b** (0.20 g, 1.13 mmol) and piperazine (0.19 g, 2.25 mmol). Pale yellow solid (0.11 g, 43%). ^{1}H NMR (400 MHz, DMSO-d_6): δ 7.79 (dd, J = 8.2, 1.4 Hz, 1H), 7.54 (dd, J = 8.4, 1.6 Hz, 1H), 7.50 (ddd, J = 8.3, 6.6, 1.4 Hz, 1H), 7.22 (ddd, J = 8.2, 6.6, 1.6 Hz, 1H), 7.09 (s, 1H), 3.63−3.56 (m, 4H), 3.16 (s, 1H), 2.80 (t, J = 4.9 Hz, 4H), 2.55 (d, J = 1.0 Hz, 3H). ^{13}C NMR (101 MHz, DMSO): δ 157.07, 147.32, 144.64, 129.04, 126.45, 123.66, 122.91, 121.68, 110.00, 45.60 (2C), 45.54 (2C), 18.54. LC−MS: $[M + H]^+$, 228.1, t_R = 1.13 min.

*1-(Pyridin-4-yl)piperazine (**28**).* The reaction was carried out following the general procedure A, using **76** (0.20 g, 1.33 mmol) and piperazine (0.23 g, 2.66 mmol). White solid (0.17 g, 78%). ^{1}H NMR (400 MHz, chloroform-*d*): δ 8.32−8.21 (m, 2H), 6.68−6.63 (m, 2H), 3.38−3.22 (m, 4H), 3.08−2.94 (m, 4H). ^{13}C NMR (101 MHz, $CDCl_3$): δ 155.44, 150.42, 108.45, 47.19 (2C), 45.84 (2C). LC−MS: $[M + H]^+$, 164.1, t_R = 0.41 min.

*1-(Naphthalen-1-yl)piperazine Monotrifluoroacetate (**29**).* K_2CO_3 (0.12 g, 0.84 mmol) was added to a solution of **77** (0.10 g, 0.70 mmol) and bis(2-chloroethyl)amine HCl (0.15 g, 0.84 mmol) in diglyme (2 mL). The resulting mixture was stirred at reflux for 48 h. The reaction mixture was cooled to room temperature, and diglyme was removed under a vacuum. The crude mixture was diluted with water and ethyl acetate and then extracted with ethyl acetate three times. The combined organic layer was dried over $MgSO_4$, filtered, and concentrated. The crude product was purified by RP-HPLC to obtain the desired product. White solid (18 mg, 7.9%). ^{1}H NMR (600 MHz, DMSO-d_6): δ 8.87 (s, 2H), 8.21−8.10 (m, 1H), 7.94−7.89 (m, 1H), 7.67 (d, J = 8.2 Hz, 1H), 7.57−7.50 (m, 2H), 7.46 (t, J = 7.8 Hz, 1H), 7.19 (dd, J = 7.5, 1.0 Hz, 1H), 3.41 (t, J = 5.0 Hz, 4H), 3.22 (s, 4H). ^{13}C NMR (151 MHz, DMSO): δ 148.11, 134.29, 128.38, 127.88, 126.09, 125.93, 125.79, 124.02, 123.18, 115.09, 49.58 (2C), 43.48 (2C). LC−MS: $[M + H]^+$, 213.2, t_R = 1.95 min.

*Quinolin-4-amine (**35**).* TFA (5 mL) was added to **78** (0.19 g, 0.95 mmol), and the mixture was stirred at room temperature overnight. The mixture was concentrated and neutralized with 1 M NaOH until the pH was ∼12. The suspension was extracted with DCM three times. The combined organic layers were dried over Na_2SO_4, filtered, and concentrated under reduced pressure. The crude was purified by silica gel column chromatography (eluting with a gradient of 0−10% MeOH in DCM) to yield the desired product. Pale yellow solid (82 mg, 60%). ^{1}H NMR (400 MHz, DMSO-d_6): δ 8.29 (d, J = 5.2 Hz, 1H), 8.13 (dd, J = 8.5, 1.4 Hz, 1H), 7.74 (dd, J = 8.5, 1.2 Hz, 1H), 7.58 (ddd, J = 8.3, 6.7, 1.4 Hz, 1H), 7.37 (ddd, J = 8.3, 6.8, 1.3 Hz, 1H), 6.74 (s, 2H), 6.53 (d, J = 5.2 Hz, 1H). ^{13}C NMR (101 MHz, DMSO): δ 151.37, 150.30, 148.76, 128.86, 128.75, 123.41, 122.27, 118.56, 102.23. LC−MS: $[M + H]^+$, 145.1, t_R = 1.28 min.

*N-Methylquinolin-2-amine (**39**).* The reaction was carried out following the general procedure A, using **75a** (0.30 g, 1.83 mmol) and methylamine solution 33 wt % in absolute ethanol (0.33 g, 0.44 mL, 3.66 mmol). White crystalline (0.24 g, 83%). ^{1}H NMR (400 MHz, DMSO-d_6): δ 7.81 (dd, J = 9.0, 0.8 Hz, 1H), 7.60 (dd, J = 7.9, 1.5 Hz, 1H), 7.51 (ddt, J = 8.3, 1.3, 0.7 Hz, 1H), 7.45 (ddd, J = 8.4, 6.8, 1.6 Hz, 1H), 7.13 (ddd, J = 8.0, 6.8, 1.3 Hz, 1H), 6.97 (q, J = 4.8 Hz, 1H), 6.74 (d, J = 8.9 Hz, 1H), 2.90 (d, J = 4.8 Hz, 3H). ^{13}C NMR (101 MHz, DMSO): δ 157.51, 147.95, 135.97, 128.91, 127.42, 125.52, 122.74, 120.96, 112.97, 27.57. LC−MS: $[M + H]^+$, 159.1, t_R = 1.49 min.

*N,N-Dimethylquinolin-2-amine (**40**).* The reaction was carried out following the general procedure A, using **75a** (0.3 g, 1.83 mmol) and dimethylamine solution 2M in MeOH (1.83 mL, 3.66 mmol). White solid (0.26 g, 82%). ^{1}H NMR (400 MHz, DMSO-d_6): δ 7.99 (dd, J = 9.2, 0.8 Hz, 1H), 7.67 (dd, J = 7.9, 1.5 Hz, 1H), 7.55 (ddt, J = 8.4, 1.4, 0.7 Hz, 1H), 7.49 (ddd, J = 8.4, 6.7, 1.6 Hz, 1H), 7.17 (ddd, J = 8.1, 6.7, 1.4 Hz, 1H), 7.07 (d, J = 9.2 Hz, 1H), 3.15 (s, 6H). ^{13}C NMR (101 MHz, DMSO): δ 157.26, 147.54, 136.98, 129.21, 127.36, 125.75, 122.08, 121.25, 109.46, 37.61 (2C). LC−MS: $[M + H]^+$, 173.1, t_R = 1.52 min.

*N-(2-Methoxyethyl)quinolin-2-amine (**41**).* The reaction was carried out following the general procedure A, using **75a** (0.30 g, 1.83 mmol) and 2-methoxyethan-1-amine (0.27 g, 3.66 mmol). Oily yellow solid (0.16 g, 43%). ^{1}H NMR (400 MHz, chloroform-*d*): δ 7.77 (dd, J = 8.9, 0.8 Hz, 1H), 7.72−7.67 (m, 1H), 7.59−7.49 (m, 2H), 7.20 (ddd, J = 8.0, 6.9, 1.2 Hz, 1H), 6.61 (d, J = 8.9 Hz, 1H), 5.16 (s, 1H), 3.77−3.71 (m, 2H), 3.66−3.61 (m, 2H), 3.39 (s, 3H). ^{13}C NMR (101 MHz, $CDCl_3$): δ 156.81, 148.00, 137.21, 129.53, 127.49, 126.23, 123.52, 122.10, 112.14, 71.51, 58.80, 41.14. LC−MS: $[M + H]^+$, 203.1, t_R = 1.61 min.

*2-(2-(Quinolin-2-ylamino)ethoxy)ethan-1-ol (**42**).* The reaction was carried out following the general procedure A, using **75a** (0.30 g, 1.83 mmol) and 2-(2-aminoethoxy)ethan-1-ol (0.38 g, 3.66 mmol). Oily off-white solid (0.11 g, 26%). ^{1}H NMR (400 MHz, chloroform-*d*): δ 7.73 (d, J = 8.9 Hz, 1H), 7.72−7.65 (m, 1H), 7.57−7.45 (m, 2H), 7.18 (ddd, J = 8.0, 6.9, 1.2 Hz, 1H), 6.59 (d, J = 8.9 Hz, 1H), 5.55 (s, 1H), 3.75 (dd, J = 5.3, 3.7 Hz, 2H), 3.71 (s, 4H), 3.60 (dd, J = 5.4, 3.6 Hz, 2H). ^{13}C NMR (101 MHz, $CDCl_3$): δ 157.00, 147.73, 137.45, 129.67, 127.52, 125.85, 123.43, 122.17, 111.88, 72.56, 70.09, 61.62, 41.41. LC−MS: $[M + H]^+$, 233.1, t_R = 1.53 min.

*N-(Quinolin-2-yl)acetamide (**43**).* A mixture of **81** (0.27 g, 1.87 mmol), 4-dimethylaminopyridine (DMAP) (0.02 g, 0.18 mmol) and triethylamine (0.28 g, 2.81 mmol) in DCM (15 mL) was stirred at 0 °C under an inert atmosphere of nitrogen. Acetyl chloride (0.18 g, 2.25 mmol) was added dropwise and resulting mixture stirred at room temperature for 2 h. A large excess methylamine [2 M in tetrahydrofuran (THF)] was then added and resulting mixture stirred for 16 h to cleave di-acetylated products. The reaction was

https://dx.doi.org/10.1021/acs.jmedchem.9b01492
J. Med. Chem. XXXX, XXX, XXX−XXX

concentrated under reduced pressure and resulting residue was purified by silica gel column chromatography (eluting with a gradient of 0−100% ethyl acetate in heptane) to obtain the desired product. White solid (0.14 g, 40%). ^{1}H NMR (400 MHz, DMSO-d_6): δ 10.80 (s, 1H), 8.37−8.26 (m, 2H), 7.89 (dd, J = 8.1, 1.5 Hz, 1H), 7.79 (dd, J = 8.4, 1.2 Hz, 1H), 7.69 (ddd, J = 8.4, 6.8, 1.5 Hz, 1H), 7.47 (ddd, J = 8.0, 6.8, 1.3 Hz, 1H), 2.15 (s, 3H). ^{13}C NMR (101 MHz, DMSO): δ 169.83, 151.72, 146.34, 138.14, 129.88, 127.70, 126.85, 125.56, 124.76, 114.22, 24.04. LC−MS: [M + H]$^+$, 187.1, t_R = 1.81 min.

*6-((4-Chlorophenoxy)methyl)quinolin-2-amine (**49**).* The reaction was carried out following the general procedure D, using **86** (0.19 g, 0.66 mmol), *tert*-butylamine (0.24 g, 3.30 mmol), and *p*-toluenesulfonic anhydride (0.43 g, 1.32 mmol). Light brown solid (46 mg, 24%). ^{1}H NMR (400 MHz, DMSO-d_6): δ 7.88 (d, J = 8.9 Hz, 1H), 7.68 (d, J = 2.0 Hz, 1H), 7.52 (dd, J = 8.6, 2.0 Hz, 1H), 7.45 (d, J = 8.5 Hz, 1H), 7.38−7.28 (m, 2H), 7.11−7.01 (m, 2H), 6.76 (d, J = 8.8 Hz, 1H), 6.44 (s, 2H), 5.14 (s, 2H). ^{13}C NMR (101 MHz, DMSO): δ 158.44, 157.25, 147.72, 136.81, 129.20 (2C), 129.12, 129.06, 126.81, 125.28, 124.30, 122.30, 116.62 (2C), 112.69, 69.68. LC−MS: [M + H]$^+$, 285.1/287.1 (Cl), t_R = 2.35 min.

*6-((4-Chlorobenzyl)oxy)quinolin-2-amine (**50**).* The reaction was carried out following the general procedure D, using **89a** (0.30 g, 1.05 mmol), *tert*-butylamine (0.38 g, 5.25 mmol), and *p*-toluenesulfonic anhydride (0.69 g, 2.10 mmol). White solid (23 mg, 7.7%). ^{1}H NMR (600 MHz, DMSO-d_6): δ 7.79 (d, J = 8.8 Hz, 1H), 7.51 (d, J = 8.5 Hz, 2H), 7.48−7.44 (m, 2H), 7.39 (d, J = 8.9 Hz, 1H), 7.23−7.17 (m, 2H), 6.73 (d, J = 8.8 Hz, 1H), 6.17 (s, 2H), 5.13 (s, 2H). ^{13}C NMR (151 MHz, DMSO): δ 156.99, 152.57, 143.37, 136.29, 136.02, 132.31, 129.49 (2C), 128.40 (2C), 126.51, 122.94, 120.50, 112.67, 108.41, 68.61. LC−MS: [M + H]$^+$, 285.1/287.1 (Cl), t_R = 2.23 min.

*6-(Benzyloxy)quinolin-2-amine (**51**).* The reaction was carried out following the general procedure D, using **89b** (0.13 g, 0.52 mmol), *tert*-butylamine (0.19 g, 2.2 mmol), and *p*-toluenesulfonic anhydride (0.34 g, 1.03 mmol). Off-white solid (20 mg, 15%). ^{1}H NMR (400 MHz, chloroform-*d*): δ 7.80 (d, J = 8.8 Hz, 1H), 7.61 (d, J = 9.1 Hz, 1H), 7.49−7.45 (m, 2H), 7.43−7.37 (m, 2H), 7.33 (td, J = 8.8, 2.2 Hz, 2H), 7.06 (d, J = 2.9 Hz, 1H), 6.71 (d, J = 8.8 Hz, 1H), 5.13 (s, 2H), 4.73 (s, 2H). ^{13}C NMR (101 MHz, $CDCl_3$): δ 155.68, 154.62, 143.02, 137.49, 137.10, 128.77 (2C), 128.17, 127.67 (2C), 127.39, 124.13, 121.98, 112.10, 108.17, 70.54. LC−MS: [M + H]$^+$, 251.1, t_R = 2.12 min.

*6-(Cyclohexylmethoxy)quinolin-2-amine (**52**).* The reaction was carried out following the general procedure D, using **89c** (0.32 g, 1.24 mmol), *tert*-butylamine (0.46 g, 6.22 mmol), and *p*-toluenesulfonic anhydride (0.81 g, 2.48 mmol). White solid (0.14 g, 44%). ^{1}H NMR (400 MHz, DMSO-d_6): δ 7.80 (d, J = 8.8 Hz, 1H), 7.36 (d, J = 8.9 Hz, 1H), 7.12 (dd, J = 9.0, 2.9 Hz, 1H), 7.08 (d, J = 2.8 Hz, 1H), 6.71 (d, J = 8.8 Hz, 1H), 6.12 (s, 2H), 3.80 (d, J = 6.3 Hz, 2H), 1.91−1.59 (m, 7H), 1.34−0.98 (m, 6H). ^{13}C NMR (101 MHz, DMSO): δ 156.80, 153.26, 143.10, 135.98, 126.38, 123.06, 120.47, 112.50, 107.61, 72.97, 37.13, 29.33 (2C), 26.05, 25.27 (2C). LC−MS: [M + H]$^+$, 257.2, t_R = 2.43 min.

*6-(4-Chlorophenyl)quinolin-2-amine (**53**).* The reaction was carried out following the general procedure D, using **92** (0.27 g, 1.06 mmol), *tert*-butylamine (0.39 g, 5.3 mmol), and *p*-toluenesulfonic anhydride (0.69 g, 2.12 mmol). Beige solid (70 mg, 26%). ^{1}H NMR (400 MHz, chloroform-*d*): δ 7.93 (d, J = 8.9 Hz, 1H), 7.81−7.75 (m, 2H), 7.72 (dd, J = 9.2, 0.7 Hz, 1H), 7.63−7.57 (m, 2H), 7.46−7.40 (m, 2H), 6.76 (d, J = 8.8 Hz, 1H), 4.84 (s, 2H). ^{13}C NMR (101 MHz, $CDCl_3$): δ 157.18, 147.34, 141.60, 139.41, 138.44, 134.46, 133.33, 129.13 (2C), 128.47 (2C), 126.71, 125.51, 123.89, 112.32. LC−MS: [M + H]$^+$, 255.1/257.1, t_R = 2.23 min.

*6-Methoxyquinolin-2-amine (**54**).* The reaction was carried out following the general procedure D, using **89d** (0.3 g, 1.71 mmol), *tert*-butylamine (0.63 g, 8.55 mmol), and *p*-toluenesulfonic anhydride (1.11 g, 3.42 mmol). Off-white solid (0.18 g, 60%). ^{1}H NMR (600 MHz, DMSO-d_6): δ 7.82 (d, J = 8.8 Hz, 1H), 7.38 (d, J = 9.0 Hz, 1H), 7.13 (dd, J = 9.0, 2.9 Hz, 1H), 7.09 (d, J = 2.9 Hz, 1H), 6.73 (d, J = 8.8 Hz, 1H), 6.16 (s, 2H), 3.79 (s, 3H). ^{13}C NMR (151 MHz, DMSO): δ 156.83, 153.77, 143.10, 136.07, 126.40, 123.02, 120.17, 112.58, 106.83, 55.22. LC−MS: [M + H]$^+$, 175.0, t_R = 1.57 min.

*6-(2-Ethoxyethoxy)quinolin-2-amine (**55**).* The reaction was carried out following the general procedure D, using **89e** (0.30 g, 1.29 mmol), *tert*-butylamine (0.47 g, 6.45 mmol), and *p*-toluenesulfonic anhydride (0.84 g, 2.58 mmol). Off-white solid (0.19 g, 63%). ^{1}H NMR (600 MHz, DMSO-d_6): δ 7.80 (d, J = 8.8 Hz, 1H), 7.38 (d, J = 9.0 Hz, 1H), 7.14 (dd, J = 9.0, 2.9 Hz, 1H), 7.11 (d, J = 2.9 Hz, 1H), 6.73 (d, J = 8.8 Hz, 1H), 6.18 (s, 2H), 4.16−4.06 (m, 2H), 3.79−3.68 (m, 2H), 3.51 (q, J = 7.0 Hz, 2H), 1.14 (t, J = 7.0 Hz, 3H). ^{13}C NMR (151 MHz, DMSO): δ 156.85, 152.94, 143.05, 136.12, 126.35, 123.00, 120.46, 112.60, 107.75, 68.39, 67.34, 65.67, 15.09. LC−MS: [M + H]$^+$, 233.1, t_R = 1.69 min.

*7-(2-Ethoxyethoxy)quinolin-2-amine (**56**).* The reaction was carried out following the general procedure D, using **89f** (0.30 g, 1.29 mmol), *tert*-butylamine (0.47 g, 6.45 mmol), and *p*-toluenesulfonic anhydride (0.84 g, 2.58 mmol). Oily pale yellow solid (49 mg, 16%). ^{1}H NMR (400 MHz, DMSO-d_6): δ 7.77 (d, J = 8.7 Hz, 1H), 7.50 (d, J = 8.7 Hz, 1H), 6.86 (d, J = 2.5 Hz, 1H), 6.79 (dd, J = 8.7, 2.5 Hz, 1H), 6.57 (d, J = 8.8 Hz, 1H), 4.14 (dd, J = 5.6, 3.7 Hz, 2H), 3.73 (dd, J = 5.4, 3.9 Hz, 2H), 3.51 (q, J = 7.0 Hz, 2H), 1.14 (t, J = 7.0 Hz, 3H). ^{13}C NMR (101 MHz, DMSO): δ 159.35, 158.55, 149.53, 136.47, 128.49, 117.46, 112.57, 109.67, 105.86, 68.29, 67.06, 65.67, 15.08. LC−MS: [M + H]$^+$, 233.1, t_R = 1.82 min.

*8-(2-Ethoxyethoxy)quinolin-2-amine (**58**).* The reaction was carried out following the general procedure D, using **89g** (0.54 g, 2.31 mmol), *tert*-butylamine (0.84 g, 11.55 mmol), and *p*-toluenesulfonic anhydride (1.51 g, 4.63 mmol). Pale yellow sold (15 mg, 2.8%). ^{1}H NMR (400 MHz, DMSO-d_6): δ 7.83 (d, J = 8.8 Hz, 1H), 7.19 (dd, J = 7.8, 1.5 Hz, 1H), 7.03 (t, J = 7.8 Hz, 1H), 6.98 (dd, J = 7.7, 1.5 Hz, 1H), 6.74 (d, J = 8.8 Hz, 1H), 6.45 (s, 2H), 4.23−4.14 (m, 2H), 3.81−3.71 (m, 2H), 3.53 (q, J = 7.0 Hz, 2H), 1.14 (t, J = 7.0 Hz, 3H). ^{13}C NMR (101 MHz, DMSO): δ 157.39, 152.13, 139.28, 136.93, 123.63, 120.84, 119.76, 112.45, 110.28, 68.46, 67.68, 65.65, 15.11. LC−MS: [M + H]$^+$, 233.1, t_R = 1.83 min.

*4-Chloroquinolin-2-amine (**60**).* The reaction was carried out following the general procedure D, using **96** (2.27 g, 12.53 mmol), *tert*-butylamine (4.58 g, 62.65 mmol), and *p*-toluenesulfonic anhydride (8.18 g, 25.05 mmol). White solid (1.10 g, 49%). ^{1}H NMR (400 MHz, DMSO-d_6): δ 7.87 (dd, J = 8.2, 1.4 Hz, 1H), 7.56 (ddd, J = 8.4, 6.7, 1.5 Hz, 1H), 7.50 (dd, J = 8.4, 1.3 Hz, 1H), 7.27 (ddd, J = 8.2, 6.7, 1.4 Hz, 1H), 6.96 (s, 1H), 6.64 (s, 2H). ^{13}C NMR (101 MHz, DMSO): δ 157.95, 148.79, 140.83, 130.35, 125.66, 123.34, 122.16, 120.30, 111.81. LC−MS: [M + H]$^+$, 179.0/181.0 (Cl), t_R = 1.67 min.

*4-(2-Ethoxyethoxy)quinolin-2-amine (**61**).* The reaction was carried out following the general procedure D, using **95a** (0.50 g, 2.14 mmol), *tert*-butylamine (0.78 g, 10.7 mmol), and *p*-toluenesulfonic anhydride (1.40 g, 4.28 mmol). Off-white solid (53 mg, 11%). ^{1}H NMR (400 MHz, DMSO-d_6): δ 7.82 (dd, J = 8.2, 1.5 Hz, 1H), 7.45 (ddd, J = 8.3, 6.7, 1.5 Hz, 1H), 7.38 (dd, J = 8.5, 1.3 Hz, 1H), 7.11 (ddd, J = 8.1, 6.7, 1.4 Hz, 1H), 6.29 (s, 2H), 6.19 (s, 1H), 4.25−4.16 (m, 2H), 3.89−3.78 (m, 2H), 3.58 (q, J = 7.0 Hz, 2H), 1.15 (t, J = 7.0 Hz, 3H). ^{13}C NMR (101 MHz, DMSO): δ 160.89, 159.36, 148.64, 129.44, 124.77, 121.24, 120.43, 116.68, 90.65, 67.92, 67.51, 65.85, 15.13. LC−MS: [M + H]$^+$, 233.2, t_R = 1.83 min.

*4-((4-Chlorobenzyl)oxy)quinolin-2-amine (**62**).* The reaction was carried out following the general procedure D, using **95b** (0.17 g, 0.59 mmol), *tert*-butylamine (0.22 g, 2.95 mmol), and *p*-toluenesulfonic anhydride (0.39 g, 1.19 mmol). White solid (30 mg, 18%). ^{1}H NMR (400 MHz, DMSO-d_6): δ 7.86 (dd, J = 8.2, 1.5 Hz, 1H), 7.57 (d, J = 8.5 Hz, 2H), 7.53−7.49 (m, 2H), 7.46 (ddd, J = 8.4, 6.7, 1.6 Hz, 1H), 7.40 (dd, J = 8.4, 1.3 Hz, 1H), 7.12 (ddd, J = 8.2, 6.7, 1.4 Hz, 1H), 6.35 (s, 2H), 6.28 (s, 1H), 5.26 (s, 2H). ^{13}C NMR (101 MHz, DMSO): δ 160.53, 159.23, 148.52, 135.34, 132.62, 129.55, 129.37 (2C), 128.55 (2C), 124.70, 121.25, 120.61, 116.67, 91.26, 68.41. LC−MS: [M + H]$^+$, 285.1/287.1 (Cl), t_R = 2.31 min.

*N^4-(4-Methoxybenzyl)quinoline-2,4-diamine (**63**).* The reaction was carried out following the general procedure B, using **60** (0.10 g, 0.56 mmol) and 4-methoxybenzylamine (0.15 g, 1.12 mmol). White

https://dx.doi.org/10.1021/acs.jmedchem.9b01492
J. Med. Chem. XXXX, XXX, XXX−XXX

solid (40 mg, 26%). ^{1}H NMR (400 MHz, DMSO-d_6): δ 7.96 (dd, J = 8.3, 1.4 Hz, 1H), 7.36 (ddd, J = 8.1, 6.7, 1.4 Hz, 1H), 7.33−7.23 (m, 4H), 7.04 (ddd, J = 8.2, 6.7, 1.5 Hz, 1H), 6.93−6.85 (m, 2H), 5.80 (s, 2H), 5.62 (s, 1H), 4.37 (d, J = 5.9 Hz, 2H), 3.72 (s, 3H). ^{13}C NMR (101 MHz, DMSO): δ 159.11, 158.13, 149.98, 148.59, 130.93, 128.46, 127.96 (2C), 125.29, 121.13, 119.32, 115.69, 113.75 (2C), 86.86, 55.01, 45.06. LC−MS: $[M + H]^+$, 280.2, t_R = 2.08 min.

*4-(Piperazin-1-yl)quinolin-2-amine (**64**).* **98** (0.2 g, 0.85 mmol) was dissolved in TFA (5 mL). The reaction mixture was heated to reflux for 3 h. The mixture was concentrated and neutralized with 1 M NaOH until the pH was ∼12. The suspension was extracted with DCM three times. The combined organic layers were dried over Na_2SO_4, filtered, and concentrated under reduced pressure. The crude was purified by silica gel column chromatography (eluting with a gradient of 0−10% MeOH in DCM) to afford the desired product. White solid (51 mg, 40%). ^{1}H NMR (600 MHz, DMSO-d_6): δ 7.72 (d, J = 8.2 Hz, 1H), 7.40 (d, J = 4.0 Hz, 2H), 7.11 (dq, J = 8.2, 4.4 Hz, 1H), 6.25 (s, 1H), 6.23 (s, 2H), 3.11−2.91 (m, 9H). ^{13}C NMR (151 MHz, DMSO): δ 158.89, 157.22, 149.34, 128.62, 125.79, 123.32, 120.24, 118.42, 99.11, 52.36 (2C), 45.17 (2C). LC−MS: $[M + H]^+$, 229.1, t_R = 0.59 min.

*4-(4-Methylpiperazin-1-yl)quinolin-2-amine (**65**).* The reaction was carried out following the general procedure B, using **60** (0.1 g, 0.56 mmol) and 1-methylpiperazine (0.11 g, 1.12 mmol). White solid (57 mg, 42%). ^{1}H NMR (400 MHz, DMSO-d_6): δ 7.70 (d, J = 8.2 Hz, 1H), 7.47−7.36 (m, 2H), 7.18−7.06 (m, 1H), 6.26 (s, 1H), 6.20 (s, 2H), 3.05 (t, J = 4.6 Hz, 4H), 2.63−2.55 (m, 4H), 2.28 (s, 3H). ^{13}C NMR (101 MHz, DMSO): δ 158.86, 156.84, 149.37, 128.56, 125.83, 123.25, 120.20, 118.44, 99.09, 54.64 (2C), 51.59 (2C), 45.71. LC−MS: $[M + H]^+$, 243.1, t_R = 0.55 min.

*1-(4-(2-Aminoquinolin-4-yl)piperazin-1-yl)ethan-1-one (**66**).* The reaction was carried out following the general procedure B, using **60** (0.11 g, 0.62 mmol) and 1-acetylpiperazine (0.16 g, 1.24 mmol). Off-white solid (95 mg, 57%). ^{1}H NMR (400 MHz, DMSO-d_6): δ 7.77 (d, J = 8.2 Hz, 1H), 7.42 (d, J = 3.8 Hz, 2H), 7.19−7.09 (m, 1H), 6.30 (s, 2H), 6.26 (s, 1H), 3.69 (dt, J = 6.6, 4.1 Hz, 4H), 3.05 (t, J = 4.9 Hz, 2H), 2.99 (t, J = 5.0 Hz, 2H), 2.06 (s, 3H). ^{13}C NMR (101 MHz, DMSO): δ 168.42, 158.68, 156.65, 149.01, 128.81, 125.62, 123.29, 120.49, 118.27, 99.34, 51.86, 51.56, 45.70, 40.88, 21.25. LC−MS: $[M + H]^+$, 271.2, t_R = 1.59 min.

*4-(Piperidin-1-yl)quinolin-2-amine (**67**).* The reaction was carried out following the general procedure B, using **60** (0.10 g, 0.56 mmol) and piperidine (0.10 g, 1.12 mmol). Off-white solid (49 mg, 38%). ^{1}H NMR (400 MHz, DMSO-d_6): δ 7.69 (d, J = 8.2 Hz, 1H), 7.44−7.37 (m, 2H), 7.10 (dq, J = 8.2, 4.4 Hz, 1H), 6.23 (s, 1H), 6.17 (s, 2H), 3.11−2.91 (m, 4H), 1.81−1.71 (m, 4H), 1.62 (q, J = 6.3 Hz, 2H). ^{13}C NMR (101 MHz, DMSO): δ 158.92, 157.82, 149.36, 128.47, 125.80, 123.28, 120.11, 118.73, 99.02, 53.04 (2C), 25.69 (2C), 24.01. LC−MS: $[M + H]^+$, 228.2, t_R = 2.15 min.

*4-Morpholinoquinolin-2-amine (**68**).* The reaction was carried out following the general procedure B, using **60** (0.10 g, 0.56 mmol) and morpholine (0.10 g, 1.12 mmol). White solid (40 mg, 31%). ^{1}H NMR (600 MHz, DMSO-d_6): δ 7.75 (d, J = 8.2 Hz, 1H), 7.46−7.38 (m, 2H), 7.16−7.06 (m, 1H), 6.27 (s, 3H), 3.84 (t, J = 4.5 Hz, 4H), 3.04 (t, J = 4.4 Hz, 4H). ^{13}C NMR (151 MHz, DMSO): δ 158.81, 156.77, 149.23, 128.71, 125.74, 123.31, 120.34, 118.23, 99.05, 66.18 (2C), 52.23 (2C). LC−MS: $[M + H]^+$, 230.1, t_R = 1.79 min.

*N^4-(2-(Dimethylamino)ethyl)quinoline-2,4-diamine (**69**).* The reaction was carried out following the general procedure B, using **60** (0.10 g, 0.56 mmol) and *N*,*N*-dimethylethylenediamine (0.10 g, 1.12 mmol). Oily brown solid (15 mg, 12%). ^{1}H NMR (400 MHz, chloroform-*d*): δ 7.93 (dd, J = 8.3, 1.5 Hz, 1H), 7.61 (dd, J = 8.5, 1.3 Hz, 1H), 7.48 (ddd, J = 8.4, 6.8, 1.5 Hz, 1H), 7.20 (ddd, J = 8.2, 6.8, 1.3 Hz, 1H), 6.18 (s, 1H), 4.87 (s, 2H), 3.32 (t, J = 6.5 Hz, 2H), 2.90 (d, J = 9.1 Hz, 5H), 2.44 (s, 3H). ^{13}C NMR (101 MHz, $CDCl_3$): δ 159.17, 157.67, 148.93, 129.55, 126.34, 124.09, 121.78, 119.84, 98.62, 55.25, 49.26, 41.32, 36.70, 1.13. LC−MS: $[M + H]^+$, 231.1, t_R = 0.55 min.

*N^4-(2-Methoxyethyl)quinoline-2,4-diamine Monotrifluoroacetate (**70**).* The reaction was carried out following the general procedure B, using **60** (0.10 g, 0.56 mmol) and 2-methoxyethylamine (0.08 g, 1.12 mmol). White solid (88 mg, 47%). ^{1}H NMR (600 MHz, DMSO-d_6): δ 12.87 (s, 1H), 8.22 (d, J = 8.3 Hz, 1H), 8.13 (t, J = 5.6 Hz, 1H), 7.82 (s, 2H), 7.69 (t, J = 7.7 Hz, 1H), 7.51 (d, J = 8.3 Hz, 1H), 7.39 (t, J = 7.7 Hz, 1H), 5.89 (s, 1H), 3.61 (t, J = 5.6 Hz, 2H), 3.48 (t, J = 5.6 Hz, 2H), 3.30 (s, 3H). ^{13}C NMR (151 MHz, DMSO): δ 154.53, 153.21, 136.75, 132.09, 123.56, 122.57, 117.60, 114.04, 82.93, 69.12, 58.17, 42.55. LC−MS: $[M + H]^+$, 218.1, t_R = 1.62 min.

*4,4′-((((Oxybis(ethane-2,1-diyl))bis(oxy))bis(ethane-2,1-diyl))bis-(oxy))bis(quinolin-2-amine) (**71**).* The reaction was carried out following the general procedure D, using **100** (0.15 g, 0.31 mmol), *tert*-butylamine (0.23 g, 3.1 mmol), and *p*-toluenesulfonic anhydride (0.40 g, 1.24 mmol). White solid (43 mg, 29%). ^{1}H NMR (400 MHz, DMSO-d_6): δ 7.81 (dd, J = 8.2, 1.5 Hz, 2H), 7.46−7.35 (m, 4H), 7.08 (ddd, J = 8.1, 6.6, 1.5 Hz, 2H), 6.25 (s, 4H), 6.17 (s, 2H), 4.19 (dd, J = 5.6, 3.5 Hz, 4H), 3.92−3.80 (m, 4H), 3.65 (td, J = 4.2, 1.1 Hz, 4H), 3.59 (td, J = 4.2, 1.2 Hz, 4H). ^{13}C NMR (101 MHz, DMSO): δ 161.30 (2C), 159.93 (2C), 149.38 (2C), 129.86 (2C), 125.40 (2C), 121.74 (2C), 120.81 (2C), 117.20 (2C), 91.15 (2C), 70.62 (2C), 70.33 (2C), 69.05 (2C), 67.91 (2C). LC−MS: $[M + H]^+$, 479.3, t_R = 1.71 min.

*4,4′-((((Oxybis(ethane-2,1-diyl))bis(oxy))bis(ethane-2,1-diyl))bis-(piperazine-4,1-diyl))bis(quinolin-2-amine) Tetratrifluoroacetate (**72**).* **101** (0.14 g, 0.19 mmol) was dissolved in TFA (5 mL). The reaction mixture was heated to reflux for 3 h. The mixture was concentrated and neutralized with 1 M NaOH until the pH was ∼12. The suspension was extracted with DCM three times. The combined organic layers were dried over Na_2SO_4, filtered, and concentrated under reduced pressure. The crude was purified by RP-HPLC to afford the desired product. White solid (20 mg, 11%). ^{1}H NMR (400 MHz, DMSO-d_6): δ 13.94 (s, 2H), 10.61 (s, 2H), 8.61 (s, 4H), 7.89 (dd, J = 8.3, 1.3 Hz, 2H), 7.75 (t, J = 7.7 Hz, 2H), 7.62 (d, J = 8.3 Hz, 2H), 7.45 (t, J = 7.7 Hz, 2H), 6.56−6.47 (m, 2H), 3.89−3.29 (m, 32H). ^{13}C NMR (101 MHz, DMSO): δ 159.22 (2C), 154.90 (2C), 137.43 (2C), 132.32 (2C), 124.99 (2C), 124.22 (2C), 118.01 (2C), 116.26 (2C), 98.21 (2C), 69.58 (4C), 69.38 (4C), 64.54 (2C), 55.09 (2C), 51.06 (2C), 48.04 (2C). LC−MS: $[M + H]^+$, 615.4, t_R = 1.25 min.

*6,6′-((((Oxybis(ethane-2,1-diyl))bis(oxy))bis(ethane-2,1-diyl))bis-(oxy))bis(quinolin-2-amine) (**73**).* The reaction was carried out following the general procedure D, using **103** (0.21 g, 0.44 mmol), *tert*-butylamine (0.32 g, 4.4 mmol), and *p*-toluenesulfonic anhydride (0.57 g, 1.76 mmol). White solid (90 mg, 43%). ^{1}H NMR (400 MHz, DMSO-d_6): δ 7.78 (d, J = 8.8 Hz, 2H), 7.37 (d, J = 9.0 Hz, 2H), 7.13 (dd, J = 9.0, 2.9 Hz, 2H), 7.09 (d, J = 2.8 Hz, 2H), 6.72 (d, J = 8.8 Hz, 2H), 6.14 (s, 4H), 4.15−4.04 (m, 4H), 3.82−3.70 (m, 4H), 3.66−3.51 (m, 8H). ^{13}C NMR (101 MHz, DMSO): δ 156.89 (2C), 152.88 (2C), 143.21 (2C), 136.02 (2C), 126.44 (2C), 123.00 (2C), 120.42 (2C), 112.57 (2C), 107.74 (2C), 69.91 (2C), 69.82 (2C), 68.97 (2C), 67.30 (2C). LC−MS: $[M + H]^+$, 479.30, t_R = 1.56 min.

*N-(4-Methoxybenzyl)quinolin-4-amine (**78**).* The reaction was carried out following the general procedure A, using **75a** (0.3 g, 1.83 mmol) and 4-methoxybenzylamine (0.50 g, 3.66 mmol). White solid (0.19 g, 39%). ^{1}H NMR (400 MHz, chloroform-*d*): δ 8.56 (dd, J = 5.3, 0.6 Hz, 1H), 8.05−7.96 (m, 1H), 7.73 (dd, J = 8.3, 1.3 Hz, 1H), 7.64 (ddd, J = 8.3, 6.9, 1.3 Hz, 1H), 7.43 (ddd, J = 8.3, 6.9, 1.3 Hz, 1H), 7.36−7.31 (m, 2H), 6.95−6.90 (m, 2H), 6.48 (d, J = 5.3 Hz, 1H), 5.22 (s, 1H), 4.46 (d, J = 5.0 Hz, 2H), 3.83 (s, 3H).

*Quinoline 1-Oxide (**80**).* The reaction was carried out following the general procedure C, using **79** (0.5 g, 3.87 mmol) and *m*-CPBA (1.00 g, 5.81 mmol). White solid (0.49 g, 87%). ^{1}H NMR (600 MHz, chloroform-*d*): δ 8.76 (dt, J = 8.8, 0.9 Hz, 1H), 8.54 (dd, J = 6.0, 1.0 Hz, 1H), 7.92−7.85 (m, 1H), 7.78 (ddd, J = 8.6, 6.9, 1.4 Hz, 1H), 7.75 (d, J = 8.3 Hz, 1H), 7.66 (ddd, J = 8.2, 6.9, 1.2 Hz, 1H), 7.30 (dd, J = 8.4, 6.0 Hz, 1H).

*Quinolin-2-amine (**81**).* The reaction was carried out following the general procedure D, using **80** (0.73 g, 5.03 mmol), *tert*-butylamine (1.84 g, 25.15 mmol), and *p*-toluenesulfonic anhydride (3.28 g, 10.06 mmol). White solid (0.29 g, 40%). ^{1}H NMR (400 MHz, DMSO-d_6): δ 7.87 (d, J = 8.8 Hz, 1H), 7.61 (dt, J = 8.0, 1.1 Hz, 1H), 7.49−7.41

https://dx.doi.org/10.1021/acs.jmedchem.9b01492
J. Med. Chem. XXXX, XXX, XXX−XXX

(m, 2H), 7.13 (ddd, J = 8.0, 5.4, 2.8 Hz, 1H), 6.75 (d, J = 8.8 Hz, 1H), 6.39 (s, 2H).

*Quinolin-6-ylmethanol (**83**).* **82** (1.00 g, 5.34 mmol) was dissolved in dry THF. $LiAlH_4$ (0.61 g, 37.95 mmol) was added slowly at −20 °C. The solution was stirred at that temperature for 1 h. Isopropanol was slowly added, and the crude filtered through Celite and washed with DCM. The filtrate was concentrated under reduced pressure. The product was used for next step without further purification. Pale yellow oil (0.80 g, 94%). ^{1}H NMR (400 MHz, DMSO-d_6): δ 8.85 (dd, J = 4.2, 1.8 Hz, 1H), 8.34 (dd, J = 8.4, 1.8 Hz, 1H), 7.97 (d, J = 8.6 Hz, 1H), 7.88 (d, J = 1.8 Hz, 1H), 7.71 (dd, J = 8.7, 1.9 Hz, 1H), 7.51 (dd, J = 8.3, 4.2 Hz, 1H), 5.40 (s, 1H), 4.70 (s, 2H).

*6-(Bromomethyl)quinoline (**84**).* **83** (0.85 g, 5.34 mmol) was dissolved in DCM (25 mL), PBr_3 (2.17 g, 8.01 mmol) was added at 0 °C slowly. The mixture was refluxed for 2 h. The mixture was concentrated under reduced pressure to give crude 6-bromomethylquinoline phosphate (1.20 g, 70%), which was used directly in the next step.

*6-((4-Chlorophenoxy)methyl)quinoline (**85**).* **84** phosphate (1.20 g, 3.75 mmol), 4-chlorophenol (0.72 g, 5.62 mmol), and K_2CO_3 (2.33 g, 16.86 mmol) were added to DMF and the mixture was heated at 80 °C under a nitrogen atmosphere until the reaction was complete by thin layer chromatography. The reaction was quenched with water, extracted with ethyl acetate three times, washed with 1 M NaOH, brine, and dried over Na_2SO_4, filtered, and concentrated under reduced pressure. The crude was purified by silica gel column chromatography (eluting with a gradient of 0−10% MeOH in DCM) to afford the desired product. White solid (0.20 g, 13%). ^{1}H NMR (400 MHz, chloroform-d): δ 8.73 (dd, J = 4.2, 1.7 Hz, 1H), 7.97 (d, J = 8.7 Hz, 1H), 7.90 (dd, J = 8.3, 1.0 Hz, 1H), 7.61 (d, J = 1.1 Hz, 1H), 7.53 (dd, J = 8.7, 2.0 Hz, 1H), 7.17 (dd, J = 8.3, 4.2 Hz, 1H), 7.09−7.02 (m, 2H), 6.78−6.70 (m, 2H), 4.95 (s, 2H).

*6-((4-Chlorophenoxy)methyl)quinoline 1-Oxide (**86**).* The reaction was carried out following the general procedure C, using **85** (0.20 g, 0.74 mmol) and *m*-CPBA (0.19 g, 1.11 mmol). White solid (0.19 g, 90%). ^{1}H NMR (400 MHz, DMSO-d_6): δ 8.58 (dd, J = 6.1, 1.0 Hz, 1H), 8.55 (d, J = 8.9 Hz, 1H), 8.14 (d, J = 1.8 Hz, 1H), 7.95 (d, J = 8.5 Hz, 1H), 7.86 (dd, J = 9.0, 1.8 Hz, 1H), 7.49 (dd, J = 8.5, 6.0 Hz, 1H), 7.39−7.32 (m, 2H), 7.14−7.05 (m, 2H), 5.33 (s, 2H).

*6-((4-Chlorobenzyl)oxy)quinoline (**88a**).* The reaction was carried out following the general procedure E, using **87a** (0.50 g, 3.44 mmol), 4-chlorobenzylbromide (0.78 g, 3.78 mmol), and K_2CO_3 (0.71 g, 5.16 mmol). White solid (0.73 g, 79%). ^{1}H NMR (400 MHz, chloroform-d): δ 8.78 (dd, J = 4.2, 1.7 Hz, 1H), 8.07−7.98 (m, 2H), 7.49−7.31 (m, 6H), 7.13 (d, J = 2.8 Hz, 1H), 5.16 (s, 2H).

*6-(Benzyloxy)quinoline (**88b**).* The reaction was carried out following the general procedure E, using **87a** (0.50 g, 3.44 mmol), benzyl bromide (0.65 g, 3.78 mmol), and K_2CO_3 (0.71 g, 5.16 mmol). Colorless oil (0.11 g, 14%). ^{1}H NMR (400 MHz, chloroform-d): δ 8.67 (dd, J = 4.3, 1.7 Hz, 1H), 7.98−7.89 (m, 2H), 7.42−7.17 (m, 7H), 7.07 (d, J = 2.8 Hz, 1H), 5.11 (s, 2H).

*6-(Cyclohexylmethoxy)quinoline (**88c**).* The reaction was carried out following the general procedure E, using **87a** (0.50 g, 3.44 mmol), (bromomethyl)cyclohexane (0.67 g, 3.78 mmol) and K_2CO_3 (0.71 g, 5.16 mmol). White solid (0.58 g, 70%). ^{1}H NMR (400 MHz, DMSO-d_6): δ 8.72 (dd, J = 4.2, 1.7 Hz, 1H), 8.23 (dd, J = 8.4, 1.7 Hz, 1H), 7.90 (d, J = 9.1 Hz, 1H), 7.45 (dd, J = 8.3, 4.2 Hz, 1H), 7.39 (dd, J = 9.1, 2.8 Hz, 1H), 7.35 (d, J = 2.8 Hz, 1H), 3.91 (d, J = 6.2 Hz, 2H), 1.93−1.59 (m, 6H), 1.36−0.98 (m, 6H).

*6-(2-Ethoxyethoxy)quinoline (**88e**).* The reaction was carried out following the general procedure E, using **87a** (1.00 g, 6.89 mmol), 1-bromo-2-ethoxyethane (1.16 g, 7.58 mmol), and K_2CO_3 (1.40 g, 10.34 mmol). Colorless oil (1.14 g, 76%). ^{1}H NMR (400 MHz, DMSO-d_6): δ 8.73 (dd, J = 4.2, 1.7 Hz, 1H), 8.23 (dd, J = 8.6, 1.7 Hz, 1H), 7.91 (d, J = 9.1 Hz, 1H), 7.47 (dd, J = 8.3, 4.2 Hz, 1H), 7.42 (dd, J = 9.1, 2.9 Hz, 1H), 7.38 (d, J = 2.8 Hz, 1H), 4.29−4.19 (m, 2H), 3.81−3.71 (m, 2H), 3.53 (q, J = 7.0 Hz, 2H), 1.15 (t, J = 7.0 Hz, 3H).

*7-(2-Ethoxyethoxy)quinoline (**88f**).* The reaction was carried out following the general procedure E, using **87b** (1.00 g, 6.89 mmol), 1-bromo-2-ethoxyethane (1.16 g, 7.58 mmol), and K_2CO_3 (1.40 g, 10.34 mmol). Orange oil (0.99 g, 66%). ^{1}H NMR (400 MHz, DMSO-d_6): δ 8.81 (dd, J = 4.3, 1.8 Hz, 1H), 8.27 (dd, J = 8.2, 1.7 Hz, 1H), 7.88 (d, J = 8.9 Hz, 1H), 7.39 (d, J = 2.6 Hz, 1H), 7.37 (dd, J = 8.2, 4.3 Hz, 1H), 7.27 (dd, J = 8.9, 2.5 Hz, 1H), 4.30−4.21 (m, 2H), 3.82−3.75 (m, 2H), 3.53 (q, J = 7.0 Hz, 2H), 1.15 (t, J = 7.0 Hz, 3H).

*8-(2-Ethoxyethoxy)quinoline (**88g**).* The reaction was carried out following the general procedure E, using **87c** (0.30 g, 2.07 mmol), 1-bromo-2-ethoxyethane (0.35 g, 2.28 mmol) and K_2CO_3 (0.43 g, 3.11 mmol). Pale yellow oil. (0.29 g, 64%). ^{1}H NMR (400 MHz, DMSO-d_6): δ 8.86 (dd, J = 4.1, 1.7 Hz, 1H), 8.30 (dd, J = 8.3, 1.8 Hz, 1H), 7.56−7.47 (m, 3H), 7.21 (dd, J = 5.4, 3.6 Hz, 1H), 4.35−4.26 (m, 2H), 3.91−3.73 (m, 2H), 3.57 (q, J = 7.0 Hz, 2H), 1.15 (t, J = 7.0 Hz, 3H).

*6-((4-Chlorobenzyl)oxy)quinoline 1-Oxide (**89a**).* The reaction was carried out following the general procedure C, using **88a** (0.73 g, 2.71 mmol) and *m*-CPBA (0.7 g, 4.06 mmol). White solid (0.66 g, 85%). ^{1}H NMR (400 MHz, DMSO-d_6): δ 8.49−8.40 (m, 2H), 7.80 (d, J = 8.5 Hz, 1H), 7.60 (d, J = 2.7 Hz, 1H), 7.55 (d, J = 8.5 Hz, 2H), 7.52−7.46 (m, 3H), 7.42 (dd, J = 8.5, 6.0 Hz, 1H), 5.27 (s, 2H).

*6-(Benzyloxy)quinoline 1-Oxide (**89b**).* The reaction was carried out following the general procedure C, using **88b** (0.11 g, 0.47 mmol) and *m*-CPBA (0.12 g, 0.70 mmol). Pale yellow solid (0.10 g, 85%). ^{1}H NMR (400 MHz, DMSO-d_6): δ 8.48−8.41 (m, 2H), 7.81 (d, J = 8.5 Hz, 1H), 7.61 (d, J = 2.7 Hz, 1H), 7.55−7.48 (m, 3H), 7.42 (ddt, J = 7.3, 6.0, 1.4 Hz, 3H), 7.39−7.33 (m, 1H), 5.26 (s, 2H).

*6-(Cyclohexylmethoxy)quinoline 1-Oxide (**89c**).* The reaction was carried out following the general procedure C, using **88c** (0.58 g, 2.40 mmol) and *m*-CPBA (0.62 g, 3.61 mmol). White solid (0.52 g, 84%). ^{1}H NMR (400 MHz, DMSO-d_6): δ 8.46−8.37 (m, 2H), 7.84−7.76 (m, 1H), 7.48 (d, J = 2.7 Hz, 1H), 7.46−7.35 (m, 2H), 3.92 (d, J = 6.1 Hz, 2H), 1.92−1.60 (m, 6H), 1.35−1.00 (m, 5H).

*6-Methoxyquinoline 1-Oxide (**89d**).* The reaction was carried out following the general procedure C, using **88d** (0.50 g, 3.14 mmol) and *m*-CPBA (0.81 g, 4.71 mmol). White solid (0.51 g, 93%). ^{1}H NMR (400 MHz, DMSO-d_6): δ 8.45−8.39 (M, 2H), 7.82 (d, J = 8.5 Hz, 1H), 7.49 (d, J = 2.7 Hz, 1H), 7.45−7.39 (m, 2H), 3.92 (s, 3H).

*6-(2-Ethoxyethoxy)quinoline 1-Oxide (**89e**).* The reaction was carried out following the general procedure C, using **88e** (1.14 g, 5.25 mmol) and *m*-CPBA (1.36 g, 7.88 mmol). White solid (1.02 g, 83%). ^{1}H NMR (400 MHz, DMSO-d_6): δ 8.45−8.42 (m, 1H), 8.42−8.40 (m, 1H), 7.82−7.76 (m, 1H), 7.51 (d, J = 2.7 Hz, 1H), 7.47−7.38 (m, 2H), 4.28−4.21 (m, 2H), 3.87−3.70 (m, 2H), 3.53 (q, J = 7.0 Hz, 2H), 1.14 (t, J = 7.0 Hz, 3H).

*7-(2-Ethoxyethoxy)quinoline 1-Oxide (**89f**).* The reaction was carried out following the general procedure C, using **88f** (0.99 g, 4.56 mmol) and *m*-CPBA (1.18 g, 6.83 mmol). White solid (0.85 g, 80%). ^{1}H NMR (400 MHz, DMSO-d_6): δ 8.55 (dd, J = 6.1, 1.0 Hz, 1H), 8.01 (d, J = 9.0 Hz, 1H), 7.91 (d, J = 2.6 Hz, 1H), 7.90−7.86 (m, 1H), 7.39 (dd, J = 9.0, 2.6 Hz, 1H), 7.33 (dd, J = 8.3, 6.1 Hz, 1H), 4.35−4.22 (m, 2H), 3.86−3.73 (m, 2H), 3.53 (q, J = 7.0 Hz, 2H), 1.14 (t, J = 7.0 Hz, 3H).

*8-(2-Ethoxyethoxy)quinoline 1-Oxide (**89g**).* The reaction was carried out following the general procedure C, using **88g** (0.29 g, 1.33 mmol) and *m*-CPBA (0.35 g, 2.00 mmol). The crude was purified by silica gel column chromatography (eluting with a gradient of 0−10% MeOH in DCM). Pale yellow oil (0.16 g, 52%). ^{1}H NMR (400 MHz, chloroform-d): δ 8.26 (d, J = 6.2 Hz, 1H), 7.48 (d, J = 8.4 Hz, 1H), 7.38−7.25 (m, 2H), 7.12−6.99 (m, 2H), 4.19 (t, J = 5.1 Hz, 2H), 3.84 (t, J = 5.1 Hz, 3H), 3.57 (q, J = 7.0 Hz, 2H), 1.13 (t, J = 7.1 Hz, 3H).

*6-(4-Chlorophenyl)quinoline (**91**).* 4-Chlorophenylboronic acid (0.23 g, 1.44 mmol), **90** (0.3 g, 1.44 mmol), K_2CO_3 (0.60 g, 4.32 mmol), $Pd(PPh_3)_4$ (33 mg, 0.0288 mmol), dioxane (30 mL), and water (6 mL) were mixed under nitrogen in a flask equipped with a reflux condenser. The reaction mixture was refluxed for 30 min. After the complete of reaction, the mixture was cooled. The solvent was removed under reduced pressure. The residue was between water and EtOAc. The aqueous phrase was then extracted by ethyl acetate three times. The organic phrase was combined, dried by Na_2SO_4, filtered,

https://dx.doi.org/10.1021/acs.jmedchem.9b01492
J. Med. Chem. XXXX, XXX, XXX−XXX

and concentrated. The crude was purified by silica gel column chromatography (eluting with a gradient of 0−100% ethyl acetate in heptane) to obtain the desired product. White solid (0.27 g, 78%). ^{1}H NMR (400 MHz, DMSO-d_6): δ 8.92 (dd, J = 4.2, 1.7 Hz, 1H), 8.44 (dd, J = 8.4, 1.8 Hz, 1H), 8.32 (t, J = 1.4 Hz, 1H), 8.10 (d, J = 1.4 Hz, 2H), 7.91−7.85 (m, 2H), 7.62−7.56 (m, 3H).

*6-(4-Chlorophenyl)quinoline 1-Oxide (**92**).* The reaction was carried out following the general procedure C, using **91** (0.27 g, 1.13 mmol) and *m*-CPBA (0.29 g, 1.69 mmol). Yellow solid (0.27 g, 93%). ^{1}H NMR (400 MHz, DMSO-d_6): δ 8.62−8.57 (m, 2H), 8.43 (d, J = 2.1 Hz, 1H), 8.15 (dd, J = 9.1, 2.1 Hz, 1H), 7.99 (d, J = 8.5 Hz, 1H), 7.92−7.86 (m, 2H), 7.64−7.59 (m, 2H), 7.51 (dd, J = 8.5, 6.0 Hz, 1H).

*4-(2-Ethoxyethoxy)quinoline (**94a**).* The reaction was carried out following the general procedure E, using **93** (0.50 g, 3.44 mmol), 1-bromo-2-ethoxyethane (0.58 g, 3.78 mmol), and K_2CO_3 (0.71 g, 5.16 mmol). Pale orange oil (0.14 g, 19%). ^{1}H NMR (400 MHz, chloroform-*d*): δ 8.74 (d, J = 5.1 Hz, 1H), 8.33−8.20 (m, 1H), 8.03 (d, J = 8.5 Hz, 1H), 7.70 (ddd, J = 8.5, 6.8, 1.6 Hz, 1H), 7.50 (ddd, J = 8.2, 6.8, 1.2 Hz, 1H), 6.74 (d, J = 5.2 Hz, 1H), 4.36 (dd, J = 5.6, 4.1 Hz, 2H), 3.99−3.92 (m, 2H), 3.67 (q, J = 7.0 Hz, 2H), 1.27 (t, J = 6.9 Hz, 3H).

*4-((4-Chlorobenzyl)oxy)quinoline (**94b**).* The reaction was carried out following the general procedure E, using **93** (0.5 g, 3.44 mmol), 4-chlorobenzylbromide (0.78 g, 3.78 mmol), and K_2CO_3 (0.71 g, 5.16 mmol). White solid (0.18 g, 19%). ^{1}H NMR (400 MHz, DMSO-d_6): δ 8.74 (d, J = 5.2 Hz, 1H), 8.18 (dd, J = 8.4, 1.5 Hz, 1H), 7.96 (dt, J = 8.4, 0.9 Hz, 1H), 7.75 (ddd, J = 8.4, 6.8, 1.5 Hz, 1H), 7.57−7.53 (m, 1H), 7.11 (d, J = 5.2 Hz, 1H), 5.40 (s, 2H).

*4-(2-Ethoxyethoxy)quinoline 1-Oxide (**95a**).* The reaction was carried out following the general procedure C, using **94a** (0.14 g, 0.64 mmol) and *m*-CPBA (0.17 g, 0.96 mmol). Pale yellow liquid (0.13 g, 87%).^{1}H NMR (400 MHz, DMSO-d_6): δ 8.53 (dd, J = 8.8, 1.2 Hz, 1H), 8.48 (d, J = 6.9 Hz, 1H), 8.19 (dd, J = 8.3, 1.4 Hz, 1H), 7.86 (ddd, J = 8.6, 6.9, 1.4 Hz, 1H), 7.75 (ddd, J = 8.2, 6.9, 1.3 Hz, 1H), 7.00 (d, J = 6.9 Hz, 1H), 4.46−4.32 (m, 2H), 3.90−3.78 (m, 2H), 3.57 (q, J = 7.0 Hz, 2H), 1.15 (t, J = 7.0 Hz, 3H).

*4-((4-Chlorobenzyl)oxy)quinoline 1-Oxide (**95b**).* The reaction was carried out following the general procedure C, using **94b** (0.18 g, 0.67 mmol) and *m*-CPBA (0.17 g, 1.01 mmol). White solid (0.17 g, 88%). ^{1}H NMR (600 MHz, DMSO-d_6): δ 8.54 (dd, J = 8.8, 1.2 Hz, 1H), 8.51 (d, J = 6.9 Hz, 1H), 8.23 (dd, J = 8.4, 1.4 Hz, 1H), 7.87 (ddd, J = 8.6, 6.9, 1.4 Hz, 1H), 7.74 (ddd, J = 8.2, 6.9, 1.2 Hz, 1H), 7.62−7.56 (m, 2H), 7.53−7.47 (m, 2H), 7.07 (d, J = 6.9 Hz, 1H), 5.40 (s, 2H).

*4-Chloroquinoline 1-Oxide (**96**).* The reaction was carried out following the general procedure C, using **74b** (2.05 g, 12.53 mmol) and *m*-CPBA (3.24 g, 18.80 mmol). White solid (2.24 g, 99%). ^{1}H NMR (400 MHz, DMSO-d_6): δ 8.62−8.56 (m, 2H), 8.24−8.19 (m, 1H), 7.97−7.86 (m, 2H), 7.70 (d, J = 6.6 Hz, 1H).

*N-(tert-Butyl)-4-chloroquinolin-2-amine (**97**).* **96** (0.27 g, 1.51 mmol) was diluted in 2:1 trifluorotoluene/DCM (5: 2.5 mL) and cooled to 0 °C. *tert*-Butylamine (0.54 g, 7.56 mmol) was added, followed by *p*-toluenesulfonic anhydride (0.98 g, 3.00 mmol) in small portions. Thirty min later, the suspension was concentrated. The crude mixture was diluted with water and DCM and then extracted with DCM three times. The combined organic layer was dried over Na_2SO_4, filtered, and concentrated. The crude product was purified by silica gel column chromatography (eluting with a gradient of 0−10% MeOH in DCM) to afford the desired product. White solid (0.20 g, 56%). ^{1}H NMR (400 MHz, DMSO-d_6): δ 7.84 (d, J = 8.2 Hz, 1H), 7.60−7.49 (m, 2H), 7.31−7.20 (m, 1H), 7.00 (s, 1H), 6.85 (s, 1H), 1.47 (s, 9H).

*N-(tert-Butyl)-4-(piperazin-1-yl)quinolin-2-amine (**98**).* The reaction was carried out following the general procedure A, using **97** (0.20 g, 0.85 mmol) and piperazine (0.15 g, 1.70 mmol). White solid (0.18 g, 75%). ^{1}H NMR (400 MHz, chloroform-*d*): δ 7.76 (dd, J = 8.2, 1.5 Hz, 1H), 7.63 (dd, J = 8.4, 1.2 Hz, 1H), 7.43 (ddd, J = 8.4, 6.8, 1.5 Hz, 1H), 7.12 (ddd, J = 8.1, 6.8, 1.3 Hz, 1H), 6.05 (s, 1H), 4.64 (s, 1H), 3.11−2.98 (m, 8H), 2.29 (s, 1H), 1.51 (s, 9H).

*4,4′-((((Oxybis(ethane-2,1-diyl))bis(oxy))bis(ethane-2,1-diyl))bis(oxy))diquinoline (**99**).* A mixture of 1,11-dibromo-3,6,9-trioxaundecane (0.30 g, 0.94 mmol), **93** (0.30 g, 2.07 mmol), and Cs_2CO_3 (0.74 g, 2.26 mmol) were added in DMF (5 mL). The mixture was allowed to stir at 80 °C for 2 h. The reaction was quenched with water, extracted with ethyl acetate three times, washed with brine, and dried over Na_2SO_4, filtered, and concentrated under reduced pressure. The crude was purified by silica gel column chromatography (eluting with a gradient of 0−10% MeOH in DCM) to afford the desired product. Pale yellow oil (0.13 g, 31%). ^{1}H NMR (400 MHz, chloroform-*d*): δ 8.66 (d, J = 5.2 Hz, 2H), 8.16 (dd, J = 8.4, 1.5 Hz, 2H), 7.98 (d, J = 8.5 Hz, 2H), 7.61 (ddd, J = 8.4, 6.8, 1.5 Hz, 2H), 7.42 (ddd, J = 8.2, 6.8, 1.2 Hz, 2H), 6.61 (d, J = 5.2 Hz, 2H), 4.22 (dd, J = 5.7, 3.9 Hz, 4H), 3.91 (dd, J = 5.6, 3.9 Hz, 4H), 3.75−3.68 (m, 4H), 3.67−3.63 (m, 4H).

*4,4′-((((Oxybis(ethane-2,1-diyl))bis(oxy))bis(ethane-2,1-diyl))bis(oxy))bis(quinoline 1-Oxide) (**100**).* The reaction was carried out following the general procedure C, using **99** (0.13 g, 0.29 mmol) and *m*-CPBA (0.15 g, 0.87 mmol). Brown oil (0.10 g, 72%). ^{1}H NMR (400 MHz, DMSO-d_6): δ 8.51 (dd, J = 8.7, 1.2 Hz, 2H), 8.47 (d, J = 6.9 Hz, 2H), 8.15 (dd, J = 8.4, 1.4 Hz, 2H), 7.83 (ddd, J = 8.6, 6.9, 1.4 Hz, 2H), 7.70 (ddd, J = 8.3, 6.9, 1.3 Hz, 2H), 6.96 (d, J = 6.9 Hz, 2H), 4.38−4.29 (m, 4H), 3.92−3.84 (m, 4H), 3.67−3.61 (m, 4H), 3.57 (td, J = 4.3, 1.4 Hz, 4H).

*4,4′-((((Oxybis(ethane-2,1-diyl))bis(oxy))bis(ethane-2,1-diyl))bis(piperazine-4,1-diyl))bis(N-(tert-Butyl)quinolin-2-amine) (**101**).* 1,11-Dibromo-3,6,9-trioxaundecane (0.10 g, 0.31 mmol), **98** (0.19 g, 0.68 mmol), and K_2CO_3 (0.13 g, 0.93 mmol) were dissolved in DMF (5 mL). The mixture was allowed to stir at room temperature for 24 h. The reaction was quenched with water, extracted with ethyl acetate three times, washed with brine, and dried over Na_2SO_4, filtered, and concentrated under reduced pressure. The crude was purified by silica gel column chromatography (eluting with a gradient of 0−10% MeOH in DCM) to afford the desired product. Pale yellow oil (0.14 g, 62%). LC−MS: $[M + H]^+$, 727.5, t_R = 1.447 min. Purity: 70%.

*6,6′-((((Oxybis(ethane-2,1-diyl))bis(oxy))bis(ethane-2,1-diyl))bis(oxy))diquinoline (**102**).* To a solution of **87a** (0.49 g, 3.37 mmol) in dry THF (45 mL) was added triphenylphosphine (1.2 g, 4.59 mmol), tetraethylene glycol (0.3 g, 1.53 mmol), and diisopropyl azodicarboxylate (DIAD) (0.92 g, 4.59 mmol). The reaction was allowed to stir at room for 72 h. The solvent was removed under reduced pressure. The crude was purified by silica gel column chromatography (eluting with a gradient of 0−10% method in DCM) to afford the desired product. Pale yellow oil (0.20 g, 29%). ^{1}H NMR (400 MHz, chloroform-*d*): δ 8.76 (dd, J = 4.3, 1.7 Hz, 2H), 8.04−7.97 (m, 4H), 7.40 (dd, J = 9.3, 2.8 Hz, 2H), 7.32 (dd, J = 8.3, 4.2 Hz, 2H), 7.05 (d, J = 2.8 Hz, 2H), 4.23 (dd, J = 5.7, 4.0 Hz, 4H), 3.95−3.90 (m, 4H), 3.79−3.70 (m, 8H).

*6,6′-((((Oxybis(ethane-2,1-diyl))bis(oxy))bis(ethane-2,1-diyl))bis(oxy))bis(quinoline 1-Oxide) (**103**).* The reaction was carried out following the general procedure C, using **102** (0.20 g, 0.45 mmol) and *m*-CPBA (0.23 g, 1.35 mmol). White solid (0.21 g, 97%). ^{1}H NMR (400 MHz, chloroform-*d*): δ 8.52 (d, J = 9.6 Hz, 2H), 8.27 (dd, J = 6.0, 1.0 Hz, 2H), 7.51−7.45 (m, 2H), 7.28 (dd, J = 9.5, 2.7 Hz, 2H), 7.12 (dd, J = 8.5, 6.0 Hz, 2H), 6.99 (d, J = 2.7 Hz, 2H), 4.20−4.09 (m, 4H), 3.90−3.80 (m, 4H), 3.71−3.60 (m, 8H).

Protein Expression and Purification. The recombinant His-tagged human p47phox^{SH3A-B} (p47phox$^{151-285}$) and p47phox^{AIR} (p47phox$^{151-342}$) (UniProtKB P14598) were cloned into a pRSET A vector and expressed in *Escherichia coli* BL21 (DE3) pLysS. p47phox^{SH3A-B} was grown in a preculture of 50 of mL LB media supplemented with 1% glucose and 100 μg/mL of ampicillin overnight (ON) at 37 °C to an approximate OD_{600} of ∼1.0. The preculture was transferred to 1 L LB-medium supplemented with 1% glucose and 100 μg/mL ampicillin and grown at 37 °C/180 rpm to an approximate OD_{600} of ∼0.5, before induction with isopropyl β-D-1-thiogalactopyranoside (IPTG) (final concentration of 0.5−1 mM) ON at 15°C/180 rpm. Cells were harvested by centrifugation at 4000*g* for 30 min. The cells were resuspended in lysis buffer (50 mM

https://dx.doi.org/10.1021/acs.jmedchem.9b01492
J. Med. Chem. XXXX, XXX, XXX−XXX

Hepes pH 7.5, cOmplete Protease Inhibitor Cocktail (1 tablet/50 mL of buffer), 25 μg/mL of DNase, 40 mM Mg_2SO_4, 150 mM NaCl, 5mM imidazole, 5% glycerol, 0.5% TritonX-100, 3 mM dithiothreitol (DTT), 1 mg/mL lysozyme) and lysed using a cell disruptor at 26 ksi in 4 °C. The cell lysate was spun down at 35,000g for 1 h at 4 °C. The supernatant was filtered on a 0.45 μm filter and loaded onto a 5 mL HisTrap HP column (GE Healthcare). The column was washed with 5 column volumes of HisTrap binding buffer (50 mM Hepes pH 7.5, 150 mM NaCl, 10 mM imidazole, 3 mM DTT) followed by eluting the protein using a gradient of HisTrap elution buffer (50 mM Hepes pH 7.5, 150 mM NaCl, 1 M imidazole, 3 mM DTT). Protein was eluted between 15 and 20% imidazole buffer and concentrated to 5 mL. The protein was loaded onto a Superdex 75 16/600 column (GE Healthcare) equilibrated with size exclusion chromatography buffer (25 mM Hepes pH 7.5, 150 mM NaCl, 1 mM TCEP) with a flow rate at 1 mL/min and was eluted at 60 mL. The protein was concentrated to 15 mg/mL and stored at −80°. The protein was analyzed on sodium dodecyl sulfate polyacrylamide gel electrophoresis for purity and concentration was measured by absorbance (NanoDrop) using molar extinction coefficient calculated based on the amino acid sequence. The exact MW of purified p47phox^{SH3A-B} was confirmed by ESI-LC/MS using an Agilent 6410 Triple Quadrupole mass spectrometer instrument coupled to an Agilent 1200 HPLC system, and using a Poroshell 300SB-C18 column (2.1 × 75 mm), and a linear gradient of the binary solvent system of water/acetonitrile/TFA (A: 95/5/0.1 and B: 5/95/0.086) with a flow rate of 1 mL/min. For proteins used in SAXS and 2D NMR studies the His-tag of p47phox^{SH3A-B} was cleaved by adding 500 μL of 1 mg/mL His-tagged human rhinovirus (HRV)-3C protease to approx. 50 mg of protein and incubated overnight at 4 °C in HisTrap binding buffer. After 16 h, the cleaved p47 protein was purified using "reverse purification" on the HisTrap HP column under the same procedure as previously described.

^{15}N-labeled p47phox^{SH3A-B} for NMR titration experiments was initially expressed in a preculture of 50 mL of LB media at 37 °C ON to an approximate OD_{600} of ∼1.0. Thirty milliliter preculture medium was centrifuged at 3500g at 37 °C for 5 min and the pellet resuspended/washed twice in 5 mL M9 minimal medium supplemented with 1 g of $^{15}NH_4Cl$ per liter of medium as the sole nitrogen source in the presence of 100 μg/mL of ampicillin and was centrifuged. The cell pellet was then resuspended in 1 L M9 minimal medium supplemented with 1 g of $^{15}NH_4Cl$ per liter and 100 μg/mL of ampicillin and grown at 37 °C/180 rpm for about 15 h to an approximate OD_{600} of ∼0.5. Protein expression was induced by adding IPTG to a final concentration of 0.5 mM at 20 °C for 24 h and cells were harvested by centrifugation at 4000g for 30 min. ^{15}N-labeled p47phox^{SH3A-B} was purified as described above for the natural abundance variant.

Fluorescence Polarization Competition Assay. The binding affinities between fluorescent peptide probes (Cy5-p22phox$^{149-162}$, TAMRA-p22phox$^{151-162}$) and p47phox^{SH3A-B} were determined as K_D values by FP saturation binding experiments. Increasing concentrations of p47phox^{SH3A-B} (two-fold dilution series, 12 points as duplicates, 0−200 μM) were added to a fixed concentration of the peptide probe (10 nM TAMRA labeled p22phox$^{151-162}$, 5 nM Cy5 labeled p22phox$^{149-16}$). The assay was performed in a HBS buffer (50 mM Hepes, 150 mM NaCl and 0.005% Tween 20, pH 7.4) using black flat-bottom 384-well plates (Corning Life Sciences, NY) and a volume of 30 μL/well. The assay plate was spun-down (33.2 g, 1 min) to ensure proper mixing and removal of potential air bubbles and incubated for 10−15 min at room temperature before measuring the FP levels on a Safire2 plate-reader (Tecan, Männedorf, Switzerland). The g-factor was adjusted at each experiment so that a series of three blank wells containing probe but no p47phox^{SH3A-B} defined the baseline FP value. The Cy5- and TAMRA-probes were measured at excitation/emission values of 635/670 and 530/585 nm, respectively. The FP values were fitted to the one-site specific binding equation: $Y = B_{max} \times X/(K_D + X)$, with B_{max} being the maximal FP value, X is the p47phox^{SH3A-B} concentration, and Y is the variable FP values. The K_D values were derived from the resulting binding saturation curve as being equal to the p47phox^{SH3A-B} concentration, where the curve is half-saturated.

The affinities between nonfluorescent peptides (p22phox$^{151-162}$, p22phox$^{149-168}$, and p22phox$^{149-162}$) or compounds and p47phox^{SH3A-B} were determined as K_i values in a heterologous competition FP binding assay. This was done by adding increasing concentration of the test compound (two-fold dilution series, 12 points as duplicates) to a fixed concentration of p47phox^{SH3A-B} (1.25 μM) and peptide probe (either 5 nM Cy5-p22phox$^{149-162}$ or 10 nM TAMRA-p22phox$^{151-162}$) using the same HBS buffer and conditions as-described above. FP values were fitted to the equation Y = bottom + (top − bottom)/[1 + ($10^{HillSlope \times (logIC_{50}-X)}$)], where X is the logarithmic value of the compound concentration. Hereby, the IC_{50} value was obtained, which together with the K_D value and probe and p47phox^{SH3A-B} concentrations was used to calculate the theoretical competitive inhibition constant, the K_i value.[39] All K_D and K_i values are reported as mean ± SEM (standard error of mean) and are based on at least three individual measurements.

The 2500 rule of 3 compliant fragments purchased from Maybridge (Thermo Fisher Scientific, US) were screened against 1.25 μM p47phox^{SH3A-B} and 5 nM Cy5-labeled p22phox$^{149-162}$ with a fragment concentration of 1 mM and a constant DMSO of 1% (v/v). p22phox$^{151-162}$ at 30 and 200 μM served as positive controls and 1% DMSO (v/v) as negative controls. Fragments that reduced the FP > 20% relative to the negative control on the respective plate were considered initial hits and selected for further validation experiments. Based on the mean mP signal of positive and negative controls, the FP screening campaign had a Z' factor of 0.83.[40] The hits found in the screening process were validated with a 6-point dose−response experiment (two-fold dilution series, as duplicates, 0.063−2 mM) in a constant 2% DMSO (v/v) HBS buffer using Cy5-p22phox$^{149-162}$ and TAMRA-p22phox$^{151-162}$ as peptide probes in separate experiments. In further dose−response validation tests with the Cy5-p22phox$^{149-162}$ probe, p47phox^{SH3A-B} was omitted from the assay to assess potential protein-independent reductions in FP indicating false-positives; and hits were tested for being aggregators by using a Triton-X containing HBS buffer (50 mM hepes, 150 mM NaCl, 0.01% Triton-X, pH 7.4).

Thermal Shift Assay. All measurements were carried out on a Stratagene Mx3005P (Agilent Technologies, Waldbronn, Germany), using clear nonskirted 96-well PCR-plates (VWR, Germany) with a sample volume of 25 μL/well. All plates were incubated for 10−15 min and spun-down for 2 min at 500 g. Protein unfolding was monitored by measuring the fluorescence of the Sypro orange (Invitrogen) fluorescent dye. The optimal protein (0.1 mg/mL, 5.8 μM) and dye concentration (8×) was determined by assessing the melting temperature of p47phox^{SH3A-B} with and without p22phox$^{151-162}$, exploring three protein concentrations (0.01, 0.1 and 1.0 mg/mL) and 12 different Sypro orange concentrations (0.5−128×), in HBS buffer and by ramping the temperature from 25 °C with increments of 1 °C/min for 55 cycles. The sigmoidal plot of the normalized FLINT values versus temperature were fitted to the Boltzman equation Y = bottom + (top − bottom)/(1 + exp((T_m − X)/slope)), where X is the temperature in °C, whereby the melting temperature (T_m) was determined as the temperature where 50% of protein is denatured.

The Maybridge library screen was performed on samples containing 0.5 mM fragments, 0.1 mg/mL (5.8 μM) p47phox^{SH3A-B} and 8× Sypro orange in 0.5% DMSO HBS buffer. Eight negative and eight positive control wells were distributed on each plate. All plates were measured starting at 30 °C with an increment of 1 °C/min for 32 cycles. Fragments able to stabilize p47phox^{SH3A-B} with a ΔT_m > 0.9 °C were considered hits and validated in a 4-point dose−response experiment (0.25−2 mM) at a constant 2% DMSO concentration. Fragments showing increasing T_m-values at across all four concentrations and with a constant fluorescence were considered validated hits. Based on the mean mP signal of positive and negative controls, the TSA screening campaign had a Z' factor of 0.62.[40]

Surface Plasmon Resonance. SPR measurements were performed at 25 °C using a Pioneer FE instrument and the data were analyzed using a Qdat Data Analysis Tool version 4.3.0 (PALL

https://dx.doi.org/10.1021/acs.jmedchem.9b01492
J. Med. Chem. XXXX, XXX, XXX−XXX

FortéBio). p47phox^{SH3A-B} was immobilized on to a biosensor chip by histidine capture followed by amine coupling using HBS pH 7.4 (10 mM Hepes, 150 mM NaCl, 0.005% tween) as immobilization and running buffer. Immobilization levels were between 2745-7010 RU p47phox^{SH3A-B}. Micro calibration (low limit 3.5% and high limit 4.5%) was performed for all SPR experiments to adjust for DMSO bulk effects. All sensorgrams were corrected for buffer bulk effects and unspecific binding of the samples to the chip matrix by blank and reference surface subtraction (subtraction of activated and inactivated blank flow cell channel).

For hit validation of screen hits and SAR analysis, the fragments were injected in five concentrations (serial dilution ranging from 63 to 2000 μM) over immobilized p47phox^{SH3A-B} using a HBS pH 7.4 running buffer supplemented with 4% DMSO using a 30 μL/min flow rate. The p22phox$^{151-162}$ peptide was used as the control before and after the experiments to evaluate activity of immobilized p47phox^{SH3A-B}. Hits from the screen showing a concentration-dependent SPR response were subsequently evaluated in an SPR inhibition assay. The dissociation constants (K_D) were estimated by plotting responses at equilibrium (R_{eq}) against the injected concentration and curve fitted to a Langmuir (1:1) binding isotherm model.

The SPR inhibition assay for initial hit validation was performed by injecting 1 mM fragments dissolved in a HBS pH 7.4 running buffer with 4% DMSO and supplemented with 10 μM p22phox$^{149-168}$ for 15 s at a 30 μL/min flow rate followed by 15 s dissociation using the 4% DMSO HBS pH 7.4 running buffer with 10 μM p22phox$^{149-168}$. Subsequently, a similar injection of 1 mM fragment over the same immobilized surface was performed using a running buffer without p22phox$^{149-168}$. p22phox$^{151-162}$ was used as the control to evaluate lack of binding in the inhibition assay. The normalized SPR response of each fragment at 13 s injection time (2 s window) with and without a blocked binding site was used to calculate metric S ($S = (R_{non\text{-}competitive} - R_{competitive})/(R_{non\text{-}competitive} + R_{competitive})$) as previously described.[28] Screening hits were considered as validated when showing both a concentration-dependent SPR response and a calculated S higher than 0.15.

The SPR competition assays for confirming competitive binding of the selected hits with p22phox$^{149-168}$ to p47phox^{SH3A-B}, were performed by immobilizing p47phox^{SH3A-B} and continuously injecting either p22phox$^{149-168}$ (10 μM) or fragments (1 mM), whilst concurrently using gradient injection (2-component injection experiments) to inject fragments or p22phox$^{149-168}$, respectively.

Nuclear Magnetic Resonance. CSP were obtain from sensitivity enhanced 2D $^{1}H-^{15}N$ HSQC spectra (hsqcetf3gpsi) recorded on Bruker AVANCE III 800 MHz or 600 MHz NMR spectrometers equipped with 5 mm TCI CryoProbes. The 2D $^{1}H-^{15}N$ HSQC spectra were acquired at 25 °C, using 200 or 256 increments and a spectra width of 2129 or 2757 Hz in the indirect dimension. A control 1D ^{1}H spectrum was recorded prior to each HSQC experiment to assess the purity and stability of the peptide/fragments. NMR sample for titration with p22phox$^{149-168}$ contained 120 μM uniformly ^{15}N-labeled p47phox^{SH3A-B} in PBS buffer (25 mM sodium phosphate buffer, 150 mM NaCl, pH 6.5.) supplemented with 5% D_2O. p22phox$^{149-168}$ was titrated at concentrations from 0 to 458 μM. NMR samples for titrations with fragments containing 150 μM uniformly ^{15}N-labeled p47phox in PBS buffer with constant 4% DMSO-d_6 (except for titration with fragment **8**, which was titrated without DMSO in the buffer) and 10% D_2O, and fragments were titrated with concentrations from 0 to 3 mM. The absolute CSP measured for the indole NH signals during titrations with each of the fragments were characterized as weak (W CSP < 1 peak width/length), medium (M CSP = 1 peak width/length), or strong (S CSP > 1 peak width/length) CSP in addition to being in fast (f) or slow (s) exchange.[41]

Small-Angle X-ray Scattering. p47phox^{SH3A-B} or p47phox^{AIR} were buffer exchanged into HBS buffer (10 mM Hepes, 150 mM NaCl, 4% DMSO, pH 7.4) without or with the presence of fragments (2, 4 or 10 mM), p22phox peptides (1 mM), or ebselen (100 or 200 μM) using Zeba Spin Desalting Columns (Thermo Fisher Scientific, 0.5 mL 7K MWCO) final protein concentrations between 2−5.6 mg/mL (130−370 μM). SAXS experiments were performed on a Xenocs BioXolver L equipped with a MetalJet X-ray source (wavelength of X-rays: 1.34 Å). We used a sample-detector distance of 654 mm, corresponding to the values of the scattering vector q between 0.01 and 0.5 Å^{-1}. Samples were automatically loaded using the sample handling robot from a 96-well tray, kept at 6 °C. Measurements were performed at room temperature. Fifteen−twenty frames (depending on the sample concentration) of 60 s exposures were collected for the protein samples, as well as for the corresponding buffers. The detector images were radially averaged. After ensuring the individual frames overlapped, they were averaged, and the buffer scattering subtracted from the sample scattering. All initial data analysis was done in software RAW.[42,43] Pair-distance distribution functions, R_g, D_{max}, and $I(0)/c$ were calculated from the scattering data using software BAYESapp.[44]

■ ASSOCIATED CONTENT

Supporting Information

The Supporting Information is available free of charge at https://pubs.acs.org/doi/10.1021/acs.jmedchem.9b01492.

Interaction of p22phox-derived peptides with p47phox^{SH3A-B} measured by FP, TSA and SPR; lack of ebselen binding to p47phox in the presence of TCEP; LC−MS of p47phox^{SH3A-B}; SPR inhibition assay of control peptide p22phox$^{151-162}$; SPR sensorgrams of fragment hits interacting with p47phox^{SH3A-B}; NMR CSPs of tryptophan-indole NH groups in p47phox^{SH3A-B} upon binding to p22phox$^{149-168}$ or fragments; solution structure of p47phox^{SH3A-B} and p47phox^{AIR} upon p22phox binding investigated by SAXS; fragments competing with p22phox$^{149-168}$ for binding to p47phox^{SH3A-B}; compound **71**−**73** tested for potential aggregation artifacts; sequence alignment of p47phox SH3A and SH3B domain; SPR steady state affinities of the p22phox-derived peptides; structural parameters obtained from SAXS of p47phox^{SH3A-B} and p47phox^{AIR}; CSPs measured for the 5 Trp indole NHs titrated with p22phox$^{149-168}$ or fragment; SPR competition assay data; and NMR and LC−MS spectra of compounds (**1**−**73**) (PDF)

Molecular formula strings (CSV)

■ AUTHOR INFORMATION

Corresponding Author

Anders Bach − *Department of Drug Design and Pharmacology, Faculty of Health and Medical Sciences, University of Copenhagen, Copenhagen 2100, Denmark;* orcid.org/0000-0003-4305-9910; Phone: +45 21288604; Email: anders.bach@sund.ku.dk

Authors

Sara Marie Øie Solbak − *Department of Drug Design and Pharmacology, Faculty of Health and Medical Sciences, University of Copenhagen, Copenhagen 2100, Denmark*

Jie Zang − *Department of Drug Design and Pharmacology, Faculty of Health and Medical Sciences, University of Copenhagen, Copenhagen 2100, Denmark*

Dilip Narayanan − *Department of Drug Design and Pharmacology, Faculty of Health and Medical Sciences, University of Copenhagen, Copenhagen 2100, Denmark*

Lars Jakobsen Høj − *Department of Drug Design and Pharmacology, Faculty of Health and Medical Sciences, University of Copenhagen, Copenhagen 2100, Denmark*

https://dx.doi.org/10.1021/acs.jmedchem.9b01492
J. Med. Chem. XXXX, XXX, XXX−XXX

Saskia Bucciarelli − *Department of Drug Design and Pharmacology, Faculty of Health and Medical Sciences, University of Copenhagen, Copenhagen 2100, Denmark*
Charlotte Softley − *Institute of Structural Biology, Helmholtz Zentrum München, Neuherberg 85764, Germany; Biomolecular NMR and Center for Integrated Protein Science Munich at Department of Chemistry, Technical University of Munich, Garching 85747, Germany*
Sebastian Meier − *Department of Chemistry, Technical University of Denmark, Kgs Lyngby 2800, Denmark;* orcid.org/0000-0003-3761-3217
Annette Eva Langkilde − *Department of Drug Design and Pharmacology, Faculty of Health and Medical Sciences, University of Copenhagen, Copenhagen 2100, Denmark;* orcid.org/0000-0003-2467-4205
Charlotte Held Gotfredsen − *Department of Chemistry, Technical University of Denmark, Kgs Lyngby 2800, Denmark*
Michael Sattler − *Institute of Structural Biology, Helmholtz Zentrum München, Neuherberg 85764, Germany; Biomolecular NMR and Center for Integrated Protein Science Munich at Department of Chemistry, Technical University of Munich, Garching 85747, Germany;* orcid.org/0000-0002-1594-0527

Complete contact information is available at: https://pubs.acs.org/10.1021/acs.jmedchem.9b01492

Author Contributions

The manuscript was written through contributions of all authors. All authors have given approval to the final version of the manuscript.

Notes

The authors declare the following competing financial interest(s): A patent application related to the results shown herein has been filed with J.Z., S.M.Ø.S., D.N. and A.B. as inventors.

■ ACKNOWLEDGMENTS

This research was supported by the Lundbeck Foundation (grant R190-2014-3710 for A.B.); the Ragna Rask Basic Research Foundation (for S.S.); the China Scholarship Council (file no. 2017062200 for J.Z.); the A. P. Møller Foundation for the Advancement of Medical Science (grant 14-28 for A.B.); the Hørslev Foundation (grant 203866-MIA for A.B.); the Augustinus Foundation (grant 14-1571 for A.B.); the Novo Nordisk Foundation SYNERGY project (grant NNF15OC0016670 for S.B.); the Lundbeck Foundation Initiative BRAINSTRUC (grant 2015-2666 for A.E.L.), and the EU Horizon 2020 Marie Skołdowska-Curie grant (grant 675555 (AEGIS) for C.S. and M.S.). We would also like to thank Dr. Kenji Ogura for kindly providing the chemical shifts of the solution NMR structure of p47phox^{SH3A-B} in complex with p22phox previously published in Ogura et al., JBC 2006.[9] We acknowledge access to NMR measurements at the Bavarian NMR Center and the NMR Center DTU, supported by the Villum Foundation.

■ ABBREVIATIONS

AIR, autoinhibitory region; CGD, chronic granulomatous disease; CSP, chemical shift perturbation; FBDD, fragment-based drug discovery; FLINT, fluorescence intensity; FP, fluorescence polarization; NADPH, nicotinamide adenine dinucleotide phosphate; NOX2, NADPH oxidase isoform 2; PAINS, pan-assay interference compounds; PKC, phosphokinase C; PRD, proline-rich domain; ROS, reactive oxygen species; SAXS, small-angle X-ray scattering; SH3, Src homology 3; SPR, surface plasmon resonance; TCEP, tris-(2-carboxyethyl)phosphine; TSA, thermal shift assay

■ REFERENCES

(1) Diebold, B. A.; Smith, S. M. E.; Li, Y.; Lambeth, J. D. NOX2 As a target for drug development: Indications, possible complications, and progress. *Antioxid. Redox Signaling* **2015**, *23*, 375−405.
(2) Block, K.; Gorin, Y. Aiding and abetting roles of NOX oxidases in cellular transformation. *Nat. Rev. Cancer* **2012**, *12*, 627−637.
(3) Bedard, K.; Krause, K.-H. The NOX family of ROS-generating NADPH oxidases: physiology and pathophysiology. *Physiol. Rev.* **2007**, *87*, 245−313.
(4) Drummond, G. R.; Selemidis, S.; Griendling, K. K.; Sobey, C. G. Combating oxidative stress in vascular disease: NADPH oxidases as therapeutic targets. *Nat. Rev. Drug Discovery* **2011**, *10*, 453−471.
(5) Bach, A. Targeting Oxidative Stress in Stroke. In *Neuroprotective Therapy for Stroke and Ischemic Disease*; Lapchak, P. A., Zhang, J. H., Eds.; Springer, 2017; pp 203−250.
(6) Groemping, Y.; Rittinger, K. Activation and assembly of the NADPH oxidase: a structural perspective. *Biochem. J.* **2005**, *386*, 401−416.
(7) El-Benna, J.; Dang, P. M.-C.; Gougerot-Pocidalo, M.-A.; Marie, J.-C.; Braut-Boucher, F. p47phox, the phagocyte NADPH oxidase/NOX2 organizer: structure, phosphorylation and implication in diseases. *Exp. Mol. Med.* **2009**, *41*, 217−225.
(8) Groemping, Y.; Lapouge, K.; Smerdon, S. J.; Rittinger, K. Molecular basis of phosphorylation-induced activation of the NADPH oxidase. *Cell* **2003**, *113*, 343−355.
(9) Ogura, K.; Nobuhisa, I.; Yuzawa, S.; Takeya, R.; Torikai, S.; Saikawa, K.; Sumimoto, H.; Inagaki, F. NMR solution structure of the tandem Src homology 3 domains of p47phox complexed with a p22phox-derived proline-rich peptide. *J. Biol. Chem.* **2006**, *281*, 3660−3668.
(10) Yuzawa, S.; Ogura, K.; Horiuchi, M.; Suzuki, N. N.; Fujioka, Y.; Kataoka, M.; Sumimoto, H.; Inagaki, F. Solution structure of the tandem Src homology 3 domains of p47phox in an autoinhibited form. *J. Biol. Chem.* **2004**, *279*, 29752−29760.
(11) Yuzawa, S.; Suzuki, N. N.; Fujioka, Y.; Ogura, K.; Sumimoto, H.; Inagaki, F. Crystallization and preliminary crystallographic analysis of the autoinhibited form of the tandem SH3 domain of p47(phox). *Acta Crystallogr., Sect. D: Biol. Crystallogr.* **2003**, *59*, 1479−1480.
(12) Yuzawa, S.; Suzuki, N. N.; Fujioka, Y.; Ogura, K.; Sumimoto, H.; Inagaki, F. A molecular mechanism for autoinhibition of the tandem SH3 domains of p47phox, the regulatory subunit of the phagocyte NADPH oxidase. *Genes Cells* **2004**, *9*, 443−456.
(13) Smith, S. M. E.; Min, J.; Ganesh, T.; Diebold, B.; Kawahara, T.; Zhu, Y.; McCoy, J.; Sun, A.; Snyder, J. P.; Fu, H.; Du, Y.; Lewis, I.; Lambeth, J. D. Ebselen and congeners inhibit NADPH oxidase 2-dependent superoxide generation by interrupting the binding of regulatory subunits. *Chem. Biol.* **2012**, *19*, 752−763.
(14) Augsburger, F.; Filippova, A.; Rasti, D.; Seredenina, T.; Lam, M.; Maghzal, G.; Mahiout, Z.; Jansen-Dürr, P.; Knaus, U. G.; Doroshow, J.; Stocker, R.; Krause, K.-H.; Jaquet, V. Pharmacological characterization of the seven human NOX isoforms and their inhibitors. *Redox Biol.* **2019**, *26*, 101272.
(15) Sakurai, T.; Kanayama, M.; Shibata, T.; Itoh, K.; Kobayashi, A.; Yamamoto, M.; Uchida, K. Ebselen, a seleno-organic antioxidant, as an electrophile. *Chem. Res. Toxicol.* **2006**, *19*, 1196−1204.
(16) Ago, T.; Nunoi, H.; Ito, T.; Sumimoto, H. Mechanism for phosphorylation-induced activation of the phagocyte NADPH oxidase protein p47(phox). Triple replacement of serines 303, 304, and 328 with aspartates disrupts the SH3 domain-mediated intramolecular interaction in p47(phox), thereby activating the oxidase. *J. Biol. Chem.* **1999**, *274*, 33644−33653.

(17) Ginsberg, M. D. Neuroprotection for ischemic stroke: past, present and future. *Neuropharmacology* **2008**, *55*, 363−389.
(18) O'Collins, V. E.; Macleod, M. R.; Donnan, G. A.; Horky, L. L.; van der Worp, B. H.; Howells, D. W. 1,026 Experimental treatments in acute stroke. *Ann. Neurol.* **2006**, *59*, 467−477.
(19) Parnham, M.; Sies, H. Ebselen: prospective therapy for cerebral ischaemia. *Expert Opin. Invest. Drugs* **2000**, *9*, 607−619.
(20) Arrowsmith, C. H.; Audia, J. E.; Austin, C.; Baell, J.; Bennett, J.; Blagg, J.; Bountra, C.; Brennan, P. E.; Brown, P. J.; Bunnage, M. E.; Buser-Doepner, C.; Campbell, R. M.; Carter, A. J.; Cohen, P.; Copeland, R. A.; Cravatt, B.; Dahlin, J. L.; Dhanak, D.; Edwards, A. M.; Frederiksen, M.; Frye, S. V.; Gray, N.; Grimshaw, C. E.; Hepworth, D.; Howe, T.; Huber, K. V. M.; Jin, J.; Knapp, S.; Kotz, J. D.; Kruger, R. G.; Lowe, D.; Mader, M. M.; Marsden, B.; Mueller-Fahrnow, A.; Müller, S.; O'Hagan, R. C.; Overington, J. P.; Owen, D. R.; Rosenberg, S. H.; Ross, R.; Roth, B.; Schapira, M.; Schreiber, S. L.; Shoichet, B.; Sundström, M.; Superti-Furga, G.; Taunton, J.; Toledo-Sherman, L.; Walpole, C.; Walters, M. A.; Willson, T. M.; Workman, P.; Young, R. N.; Zuercher, W. J. The promise and peril of chemical probes. *Nat. Chem. Biol.* **2015**, *11*, 536−541.
(21) Azad, G. K.; Tomar, R. S. Ebselen, a promising antioxidant drug: mechanisms of action and targets of biological pathways. *Mol. Biol. Rep.* **2014**, *41*, 4865−4879.
(22) Congreve, M.; Carr, R.; Murray, C.; Jhoti, H. A "rule of three" for fragment-based lead discovery? *Drug Discovery Today* **2003**, *8*, 876−877.
(23) Feng, B. Y.; Shoichet, B. K. A detergent-based assay for the detection of promiscuous inhibitors. *Nat. Protoc.* **2006**, *1*, 550−553.
(24) Turek-Etienne, T. C.; Small, E. C.; Soh, S. C.; Xin, T. A.; Gaitonde, P. V.; Barrabee, E. B.; Hart, R. F.; Bryant, R. W. Evaluation of fluorescent compound interference in 4 fluorescence polarization assays: 2 kinases, 1 protease, and 1 phosphatase. *J. Biomol. Screening* **2003**, *8*, 176−184.
(25) Hubbard, R. E.; Murray, J. B. Experiences in fragment-based lead discovery. *Methods Enzymol.* **2011**, *493*, 509−531.
(26) Schiebel, J.; Radeva, N.; Köster, H.; Metz, A.; Krotzky, T.; Kuhnert, M.; Diederich, W. E.; Heine, A.; Neumann, L.; Atmanene, C.; Roecklin, D.; Vivat-Hannah, V.; Renaud, J.-P.; Meinecke, R.; Schlinck, N.; Sitte, A.; Popp, F.; Zeeb, M.; Klebe, G. One question, multiple answers: Biochemical and biophysical screening methods retrieve deviating fragment hit lists. *ChemMedChem* **2015**, *10*, 1511−1521.
(27) Wielens, J.; Headey, S. J.; Rhodes, D. I.; Mulder, R. J.; Dolezal, O.; Deadman, J. J.; Newman, J.; Chalmers, D. K.; Parker, M. W.; Peat, T. S.; Scanlon, M. J. Parallel screening of low molecular weight fragment libraries: do differences in methodology affect hit identification? *J. Biomol. Screening* **2013**, *18*, 147−159.
(28) Giannetti, A. M.; Gilbert, H. N.; Huddler, D. P.; Reiter, M.; Strande, C.; Pitts, K. E.; Bravo, B. J. Chapter 2: Getting the Most Value from Your Screens: Advances in Hardware, Software, and Methodologies to Enhance Surface Plasmon Resonance Based Fragment Screening and Hit-to-Lead Support. In *Fragment-Based Drug Discovery*; Royal Society of Chemistry, 2015; pp 19−48.
(29) Lagorce, D.; Bouslama, L.; Becot, J.; Miteva, M. A.; Villoutreix, B. O. FAF-Drugs4: free ADME-tox filtering computations for chemical biology and early stages drug discovery. *Bioinformatics* **2017**, *33*, 3658−3660.
(30) Irwin, J. J.; Duan, D.; Torosyan, H.; Doak, A. K.; Ziebart, K. T.; Sterling, T.; Tumanian, G.; Shoichet, B. K. An aggregation advisor for ligand discovery. *J. Med. Chem.* **2015**, *58*, 7076−7087.
(31) Quinn, J. G. Evaluation of Taylor dispersion injections: determining kinetic/affinity interaction constants and diffusion coefficients in label-free biosensing. *Anal. Biochem.* **2012**, *421*, 401−410.
(32) Quinn, J. G. Modeling Taylor dispersion injections: determination of kinetic/affinity interaction constants and diffusion coefficients in label-free biosensing. *Anal. Biochem.* **2012**, *421*, 391−400.
(33) Inglis, S.; Jones, R.; Fritz, D.; Stojkoski, C.; Booker, G.; Pyke, S. Synthesis of 5-, 6- and 7-substituted-2-aminoquinolines as SH3 domain ligands. *Org. Biomol. Chem.* **2005**, *3*, 2543−2557.
(34) Inglis, S. R.; Stojkoski, C.; Branson, K. M.; Cawthray, J. F.; Fritz, D.; Wiadrowski, E.; Pyke, S. M.; Booker, G. W. Identification and specificity studies of small-molecule ligands for SH3 protein domains. *J. Med. Chem.* **2004**, *47*, 5405−5417.
(35) Jones, R. Investigating 2-Aminoquinoline Derivatives as Small Molecule Ligands for the Tec SH3 Domain. Ph.D. Thesis, University of Adelaide, 2007.
(36) Pulido, D.; Casadó-Anguera, V.; Pérez-Benito, L.; Moreno, E.; Cordomí, A.; López, L.; Cortés, A.; Ferré, S.; Pardo, L.; Casadó, V.; Royo, M. Design of a true bivalent ligand with picomolar binding affinity for a G protein-coupled receptor homodimer. *J. Med. Chem.* **2018**, *61*, 9335−9346.
(37) Bach, A.; Chi, C. N.; Pang, G. F.; Olsen, L.; Kristensen, A. S.; Jemth, P.; Strømgaard, K. Design and synthesis of highly potent and plasma-stable dimeric inhibitors of the PSD-95-NMDA receptor interaction. *Angew. Chem., Int. Ed.* **2009**, *48*, 9685−9689.
(38) Zielonka, J.; Cheng, G.; Zielonka, M.; Ganesh, T.; Sun, A.; Joseph, J.; Michalski, R.; O'Brien, W. J.; Lambeth, J. D.; Kalyanaraman, B. High-throughput assays for superoxide and hydrogen peroxide: design of a screening workflow to identify inhibitors of NADPH oxidases. *J. Biol. Chem.* **2014**, *289*, 16176−16189.
(39) Nikolovska-Coleska, Z.; Wang, R.; Fang, X.; Pan, H.; Tomita, Y.; Li, P.; Roller, P. P.; Krajewski, K.; Saito, N. G.; Stuckey, J. A.; Wang, S. Development and optimization of a binding assay for the XIAP BIR3 domain using fluorescence polarization. *Anal. Biochem.* **2004**, *332*, 261−273.
(40) Zhang, J.-H.; Chung, T. D.; Oldenburg, K. R. A simple statistical parameter for use in evaluation and validation of high throughput screening assays. *J. Biomol. Screening* **1999**, *4*, 67−73.
(41) Williamson, M. P. Using chemical shift perturbation to characterise ligand binding. *Prog. Nucl. Magn. Reson. Spectrosc.* **2013**, *73*, 1−16.
(42) Hopkins, J. B.; Gillilan, R. E.; Skou, S. BioXTAS RAW: improvements to a free open-source program for small-angle X-ray scattering data reduction and analysis. *J. Appl. Crystallogr.* **2017**, *50*, 1545−1553.
(43) Nielsen, S. S.; Toft, K. N.; Snakenborg, D.; Jeppesen, M. G.; Jacobsen, J. K.; Vestergaard, B.; Kutter, J. P.; Arleth, L. BioXTAS RAW, a software program for high-throughput automated small-angle X-ray scattering data reduction and preliminary analysis. *J. Appl. Crystallogr.* **2009**, *42*, 959−964.
(44) Hansen, S. BayesApp: a web site for indirect transformation of small-angle scattering data. *J. Appl. Crystallogr.* **2012**, *45*, 566−567.

https://dx.doi.org/10.1021/acs.jmedchem.9b01492
J. Med. Chem. XXXX, XXX, XXX−XXX